Primitive-Equation-Based Low-Order Models with Seasonal Cycle. I. Model Construction

Ulrich Achatz

Leibniz-Institut für Atmosphärenphysik an der Universität Rostock

Kühlungsborn, Germany

J.D. Opsteegh

KNMI, De Bilt, The Netherlands

submitted to *J. Atmos. Sci.* June 17, 2001

revised April 2, 2002

Abstract

In a continuation of previous investigations on deterministic reduced atmosphere models with compact state space representation (Achatz and Branststor, 1999) two main modifications are introduced: First, primitive-equation dynamics is used to describe the nonlinear interactions between resolved scales. Secondly, the seasonal cycle in its main aspects is incorporated. Stability considerations lead to a grid-point formulation of the basic equations in the dynamical core. A total energy metric consistent with the equations can be derived, provided surface pressure is treated as constant in time. Using this metric, a reduction in the number of degrees of freedom is achieved by a projection onto three-dimensional EOFs, each of them encompassing simultaneously all prognostic variables (winds and temperature). The impact of unresolved scales and not explicitely described physical processes is incorporated via an empirical linear parameterization. The basis patterns having been determined from three sigma levels from a GCM data set, it is found that, in spite of the presence of a seasonal cycle, at most 500 are needed for describing 90% of the variance produced by the GCM. If compared to previous low-order models with quasi-geostrophic dynamics our reduced models exhibit at this and lower-order truncations a considerably enhanced capability to predict GCM tendencies. An analysis of the dynamical impact of the empirical parameterization is given, hinting to an important role in controlling the seasonally-dependent storm-track dynamics.

1 Introduction

The development of a reduced model of atmospheric dynamics is an attempt at explicitely dealing only with the essential degrees of freedom represented by the climate attractor while still not giving away much realism in comparison to nature or standard general circulation models (GCM). A basis of near-optimal patterns is used which span about every conceivable atmospheric state-vector while simultaneously ignoring improbable cases. The low-order model for the corresponding expansion coefficients provides an interesting practical test of the complexity of the climate attractor.

Besides this more fundamental motivation, and a rather distant aim to eventually also use reduced models in climate change studies, the main incentive for their development originates from the hope that they might serve as improved substitutes for traditional low-order models. Due to an ever decreasing comprehensibility of specific simulation results from the most realistic GCMs, these have always been important tools scientists have resorted to when the understanding of fundamental dynamical processes was the aim (e.g. Lorenz, 1963; Charney and DeVore, 1979; Legras and Ghil, 1985; Vautard and Legras, 1988; Michelangeli et al., 1995; Hannachi, 1997). However, they have shared the weakness of either being only in qualitative agreement with nature or focussing on special areas of the globe. It could be interesting to set some of the lessons we have learned from low-order models on firmer ground by using more realistic reduced models. Furthermore, enhanced realism might also facilitate the study of new problems which have so far been out of reach for low-order modelling.

For clarification, a few words might be added on what we mean by a reduced model. Clearly, this term already seems justified if applied to any model using simplifications which go farther than traditional spatial filtering, e.g. by severe spectral truncation, or

dynamical filtering, as e.g. done in quasi-geostrophic models. A very interesting work in this regard has been published by Moise and Temam (2000) who outline a general strategy for using group renormalization methods in reductions of the incompressible Navier-Stokes equations. A considerable way might however still be left until their concepts can be applied to the primitive equations on a sphere. Another important class of dynamical simplifications is represented by linear models supplemented by stochastic forcing. They have been quite successful in the description of several aspects of the climate system, be it atmospheric transient-eddy activity (e.g. Farrell and Ioannou, 1993, 1994; Whitaker and Sardeshmukh, 1998; DelSole and Hou, 1999; Zhang and Held, 1999) or tropical SST variability (Penland and Matrosova, 1994; Penland and Sardeshmukh, 1995). Here it is interesting to note that, in some cases, it was not only the parameterization of the nonlinear impact by linear damping and additive noise which led to an especially simple description. Additionally, the use of a basis of empirical orthogonal functions (EOF) also provided a state space compression which goes far beyond the reaches of traditional spectral expansions.

This brings us to our personal definition of a reduced model: Irrespective of the dynamical equations employed *it should contain a state space description using as few degrees of freedom as possible while retaining realism and comprehensiveness.* Given a certain low number of degrees of freedom this is to be achieved by (1) the use of optimal basis patterns and (2) suitable parameterizations of the impact of unresolved scales and processes. Varying within this framework the number of basis patterns can then yield insights into the overall complexity of the atmosphere. Furthermore, we want to have a model formulation which can describe in some sense the impact of changes in the large-scale state of the system onto its local linear dynamics and onto the nonlinear, fluctuating,

forcing of the larger scales by the smaller ones. In the context of stochastic modelling this seems to be a difficult problem which is just beginning to be mastered (DelSole, 2001). Therefore we focus here on reduced models which are *nonlinear and deterministic*.

In practice the optimal basis is approximated by some near-optimal set. While traditional spherical harmonics are not well suited for this purpose, interesting candidates are principal interaction patterns (PIP; Hasselmann, 1988) and EOFs. The latter, although being less optimal than PIPs (Kwasniok, 1996, 1997; Achatz and Schmitz, 1997) have the advantage that they are obtained with relatively little work. Moreover, they have been shown to serve reasonably well as a basis of reduced atmosphere models (e.g. Rinne and Karhilla, 1975; Selten, 1995, 1997a,b; Achatz and Branstator, 1999; d'Andrea and Vautard, 2001). Another interesting alternative has recently been suggested by Farrell and Ioannou (2001). They discuss truncations of the dynamics of linear models in Hankel representation which, due to their incorporation of the leading stochastic optimals into the reduced basis, might enhance the ability of the simplified model to correctly respond to external perturbations. They have, however, not yet shown how their method can lead to deterministic nonlinear reduced models. This special case being the very focus of our work we have therefore chosen to concentrate for the present on EOF models and to try to learn as much as possible from those, for later times losing the option of even more advanced approaches not out of sight.

Within the context of EOF-modelling a promising strategy is the use of semi-empirical models. These are obtained by projecting an approximate, but still resasonable, dynamical model for the prognostic fields (the dynamical model core) onto the basis patterns and extracting a parameterization of the impact of unresolved scales and not explicitely described processes by empirical means from some reference data set. An interesting re-

sult by Achatz and Branstator (1999, henceforth called AB) has been that such an EOF model, based on a quasigeostrophic two-layer model core and closed with an empirically determined linear parameterization, is reproducing not only the mean state and transient fluxes but also the leading variance patterns from a perpetual January GCM integration. Furthermore, shedding some light on the complexity of the GCM's attractor, it was observed that in many respects a model based on as few as 30 patterns was already behaving in a correct manner, while 500 patterns were necessary to represent the daily weather at sufficient accuracy.

Nonetheless, some limitations of this work must be recognized. First, both GCM and reduced models did not simulate the seasonal cycle. Secondly, even for the larger EOF model with 500 basis patterns the local tendency errors were still considerable (about 50%). Finally, the reduced models did not respond correctly to anomalous local heating in the tropics. The second problem could possibly be traced back to the use of a quasi-geostrophic model core for the global nonlinear dynamics. Even the third problem might, at least in parts, be due to this deficiency. Before resorting to farther-going alternatives as e.g. trying a basis with stochastic optimals, as suggested by Farrell and Ioannou (2001), it therefore seemed worthwhile to first extend the realism of semi-empirical EOF models by incorporating seasonality and primitive-equation dynamics.

We have set out to work in this direction, using for the determination of the EOFs and the empirical closure a 2000-year long data set of the atmospheric part of a coupled atmosphere/ocean GCM. Section 2 gives an overview of semi-empirical reduced models. Section 3 introduces the primitive-equation dynamical model core. In section 4 the determination of global EOFs from the data set is discussed. Section 5 describes the extraction of the empirical closure from the data, analyzes its impact on the predictability of GCM

tendencies by our models, and examines how this impact is achieved. Section 6 summarizes and discusses the results. Investigations of the ability of the models to predict the GCM over shorter periods and simulate its climate will be reported in a companion paper, along with an application to weather regimes.

2 Semi-empirical reduced models in general

2.1 Projected model

Reduced models are intended for the compact description of the behaviour of complex systems (e.g. a GCM or the atmosphere itself) with a very large number of variables. Concentrating among those on n variables of prior interest (the *primary state*, typically flow field and temperature at a not too fine horizontal resolution and on a limited number of levels), the corresponding state vector $\mathbf{X} \in \mathcal{R}^n$ is expanded as

$$\mathbf{X}(t) = \mathbf{X}^r + \sum_{\nu=1}^{N} a_\nu(t)\mathbf{e}^\nu + \boldsymbol{\rho}(t)\,, \tag{1}$$

in terms of $N \ll n$ orthonormal basis vectors $\mathbf{e}^\nu$ so that the residual error $\boldsymbol{\rho}$ (comprising all components of the primary state which will not be resolved in the reduced model) is near to its possible absolute minimum, if averaged over all states on the attractor (assuming stationarity). $\mathbf{X}^r$ denotes a reference state which in many cases is chosen to be some long-time mean of the primary state vector. The degrees of freedom in a reduced model are the expansion coefficients $a_\nu(t)$ which can be obtained from the primary state vector by means of a suitably defined scalar product:

$$a_\nu(t) \;\; = \;\; (\mathbf{e}^\nu, \mathbf{X}(t) - \mathbf{X}^r) \tag{2}$$

For the sake of simplicity we want to use as basis patterns EOFs which can be obtained from a sufficiently large number of observations of the system in a rather straightforward

manner: If $\mathsf{S} = \overline{(\mathbf{X}-\overline{\mathbf{X}})(\mathbf{X}-\overline{\mathbf{X}})^T}$ is the lag-zero covariance matrix (overbars indicate averaging over all data) then the EOFs are solutions of the eigenvalue problem $\mathsf{SM}\mathbf{e}^\nu = \lambda_\nu^2 \mathbf{e}^\nu$. M is the metric defining the scalar product. If $\mathbf{X}^r = \overline{\mathbf{X}}$ the residual error in (1) is minimized by picking those N patterns with the largest eigenvalues, i.e. variances explained.

Although already the choice of a reduced basis is not obvious, this holds even less for the specification of the dynamical equations of the reduced model. One must choose some set of functions $r_\nu(\mathbf{a})$ so that solution of $\dot{\mathbf{a}} = \mathbf{r}(\mathbf{a})$ yields a good approximation of the true time-dependence of the vector $\mathbf{a}$ of expansion coefficients. As has been shown (Achatz and Schmitz, 1997; Selten, 1997b; Achatz and Branstator, 1999), such a model can be obtained by a strategy consisting of two parts. In the first step one takes approximate tendencies $\mathbf{g}(\mathbf{X})$ for the primary state (henceforth called the *dynamical model core*), based on the fundamental geophysical fluid-dynamical equations, and uses it for calculating the interaction between the resolved components. In the second step one resorts to empirical means for obtaining a parameterization of the impact of all unresolved components and of all physical processes which are not described by the dynamical core. The dynamical core should be good enough so that, for all states on the attractor, the residue $\dot{\mathbf{X}}-\mathbf{g}(\mathbf{X})$ between the true tendencies and their approximation is small. As an example, if the primary state only consists of streamfunction variables the appropriate dynamical equations could be taken from a quasigeostrophic model. Projecting the true tendencies onto the basis patterns, with the help of (1) and (2), yields for the tendencies of the expansion coefficients

$$\dot{a}_\nu = t_\nu(\mathbf{a}) + \Delta_\nu(\mathbf{a}, \boldsymbol{\rho}, \mathbf{Y}) \tag{3}$$

where the time derivatives of the *projected model* are given by

$$t_\nu(\mathbf{a}) = (\mathbf{e}^\nu, \mathbf{g}(\mathbf{X}^r + \sum_{\nu=1}^{N} a_\nu(t)\mathbf{e}^\nu))\,, \tag{4}$$

and $\Delta_\nu(\mathbf{a}, \boldsymbol{\rho}, \mathbf{Y}) = (\mathbf{e}^\nu, \dot{\mathbf{X}}(\mathbf{X}, \mathbf{Y})) - t_\nu(\mathbf{a})$ represents the impact of the unresolved components, which are given by $\boldsymbol{\rho}$, and the vector $\mathbf{Y}$ comprising all system variables in the subspace orthogonal to the primary state space.

Clearly, the metric is important, both for the determination of the EOFs, and for the model projection. Our decision for the corresponding choice is influenced by two considerations. The first has to do with stability issues: If, as is often the case, the dynamical model core can be written

$$g_i(\mathbf{X}) = F_i^X + \sum_{j=1}^{n} L_{ij}^X X_j + \sum_{j=1}^{n}\sum_{k=1}^{n} N_{ijk}^X X_j X_k \tag{5}$$

with external forcing $\mathbf{F}^X$, and linear and nonlinear interaction tensors L^X and N^X, respectively, then projection yields

$$t_\nu(\mathbf{a}) = F_\nu + \sum_{\mu=1}^{N} L_{\nu\mu} a_\mu + \sum_{\mu=1}^{N}\sum_{\rho=1}^{N} N_{\nu\mu\rho} a_\mu a_\rho \tag{6}$$

where the projected model's forcing, its linear tensor, and its nonlinear tensor are each given by

$$F_\nu = \sum_{i=1}^{n} e_i^\nu \sum_{j=1}^{n} M_{ij} g_j(\mathbf{X}^r) \tag{7}$$

$$L_{\nu\mu} = \sum_{i=1}^{n} e_i^\nu \sum_{j=1}^{n} M_{ij} \sum_{k=1}^{n} \left[L_{jk}^X e_k^\mu + \sum_{l=1}^{n} N_{jkl}^X \left(e_k^\mu X_l^r + e_l^\mu X_k^r \right) \right] \tag{8}$$

$$N_{\nu\mu\rho} = \sum_{i=1}^{n} e_i^\nu \sum_{j=1}^{n} M_{ij} \sum_{k=1}^{n}\sum_{l=1}^{n} N_{jkl}^X e_k^\mu e_l^\rho. \tag{9}$$

It is interesting to note that nonlinear instabilities (Phillips, 1959) are not automatically excluded if any metric is chosen for the projection. It might happen that the nonlinear terms obtained from (9) create energy leading to unbounded growth. Avoidance of this potential pitfall is desirable whenever possible. It has been shown by AB that *if* (1) the dynamical model core $\dot{\mathbf{X}} = \mathbf{g}(\mathbf{X})$ conserves total energy, (2) total energy can be written as a quadratic function of the variables, i.e. $E = \mathbf{X}^T \mathsf{M}^E \mathbf{X}$, with the total energy metric

M^E being a positive definite symmetric matrix, (3) the nonlinear terms in $\mathbf{g}(\mathbf{X})$ are of polynomial form, and (4) the basis patterns are orthonormal with respect to the total energy metric, i.e. $\mathbf{e}^{\nu T}\mathsf{M}^E\mathbf{e}^{\mu} = \delta_{\nu\mu}$, *then* projection of $\mathbf{g}(\mathbf{X})$ onto the basis patterns using this metric yields nonlinear terms in the model which conserve turbulent energy $\mathbf{a}^T\mathbf{a}$. In the case of quadratic nonlinearities this is due to the satisfaction of the triad condition $\sum_{perm(\nu,\mu,\rho)} N_{\nu\mu\rho} = 0$.

This is a somewhat complex argument in favor of taking $\mathsf{M} = \mathsf{M}^E$. The other one is of a more obvious kind: In performing the EOF analysis weights have to be assigned to variables which are of different physical character, as is the case for temperatures and velocities. This must again be decided by specifying the most appropriate metric. Here the total energy metric is a dynamically plausible choice since the weight it gives to each of the variables is the total energy variance associated with it. We are therefore using a total energy metric in our work. How this can be done in the primitive-equation context is discussed in section 3.

2.2 Empirical closure and dissipation tuning

In the second step of the semi-empirical approach an attempt is made to express the impact of the unresolved components onto the resolved part as a function of the reduced model variables alone, i.e. to derive a function $\delta_\nu(\mathbf{a}, \boldsymbol{\alpha}) \approx \Delta_\nu(\mathbf{a}, \boldsymbol{\rho}, \mathbf{Y})$ where $\boldsymbol{\alpha}$ is a vector of constant closure parameters. The approximate equality should hold in some reasonable average sense. Derivation of such a parameterization from the basic geophysical fluid-dynamical equations by purely analytical means is a tremendous task. A way to do so might have been indicated by Moise and Teman (2000) but considerable work could still be necessary to develop their method far enough for applicability to our purposes. We

resort therefore to a more practical approach, i.e. specification of a functional form for all δ_ν, and empirical extraction of the closure parameters from a dataset with sufficiently many observations of $\mathbf{X}$ and its tendencies. This is done by minimizing the mean relative error between model tendencies and their observed counterparts,

$$\epsilon_t = \frac{\overline{\sum_{\nu=1}^{N}[(\mathbf{e}^\nu, \dot{\mathbf{X}}) - t_\nu(\mathbf{a}) - \delta_\nu(\mathbf{a}, \boldsymbol{\alpha})]^2}}{\overline{\sum_{\nu=1}^{N}(\mathbf{e}^\nu, \dot{\mathbf{X}})^2}} \,. \tag{10}$$

It is understood that for each observation $\mathbf{a}$ is calculated from $\mathbf{X}$ by use of (2). An alternative to minimizing tendency errors could be the fitting of short trajectories of the reduced model to the observed ones as has e.g. been done by Kwasniok (1997).

Interrupting the so-far general presentation, in order to give some illustration, let us shortly provide the reader with the specific form of closure we have used in this work. Motivated by the result in AB that a linear ansatz can do quite well, we have tried this approach also here. One modification was necessary, viz. we had to make the closure parameters slowly time-dependent, in order to enable the model to reproduce the correct seasonal dependence of mean state and fluxes. We have thus set

$$\delta_\nu(\mathbf{a}, \boldsymbol{\alpha}) \;=\; \mathbf{F}(t) + \mathsf{L}(t)\mathbf{a} \tag{11}$$

with

$$\mathbf{F}(t) \;=\; \mathbf{F}_0 + \sum_{n=1}^{2} [\mathbf{F}_n^c \cos(n\Omega t) + \mathbf{F}_n^s \sin(n\Omega t)] \tag{12}$$

$$\mathsf{L}(t) \;=\; \mathsf{L}_0 + \sum_{n=1}^{2} [\mathsf{L}_n^c \cos(n\Omega t) + \mathsf{L}_n^s \sin(n\Omega t)] \,. \tag{13}$$

Here Ω is the angular frequency of the earth's circumsolar orbit. The parameter vector to be adjusted in the tendency error minimization contains the coefficients of $\mathbf{F}_0, \mathbf{F}_n^{c,s}(n = 1, 2), \mathsf{L}_0$, and $\mathsf{L}_n^{c,s}(n = 1, 2)$. In an initial attempt we had also tried a parameterization with time-independent linear operator. The resulting model failed, however, in producing a seasonal dependence of the transient fluxes.

Experience has shown that empirical determination of the closure parameters by the above-described method is sufficient if the reduced model equations can predict the true tendencies very accurately (Achatz and Schmitz, 1997). However, if the relative tendency error after minimization is still not negligible, typically the model's dissipation is not tuned well yet so that it tends to be too energetic when integrated. Some a posteriori tuning of a suitably defined, in general very weak, damping must therefore be performed in addition [1].

More specifically, we add to the tendency of each EOF an additional newtonian damping $-h_\nu[a_\nu - a_\nu^s(t)]$ with

$$h_\nu = A\left(\frac{\nu}{N}\right)^\beta . \tag{14}$$

$a_\nu^s(t)$ is the seasonally dependent climate mean, represented, just as the closure terms, by a constant part, an annual component, and a semi-annual component, all of them estimated from the reference data set. The constants A and β have been determined for

[1] This can be done by two different methods outlined in AB. The first relies on results by Penland and Sardeshmukh (1995, Appendix A), DelSole (1996), and AB (Appendix D) where it is shown how the damping described by a linear tensor depends on whether true total tendencies (or their relatively precise central-difference estimates from the data set) are used in its empirical determination, or tendencies estimated from forward differences with nonnegligible time difference. AB have made use of this dependence and employed a mixture of central differences and forward differences in the determination of the closure. The corresponding mixing parameter was varied in the tuning, i.e. it was optimized so that the climate of the reduced model and that of the GCM agreed as well with each other as possible. The second approach tested by AB is taking central differences in the calculation of the relative tendency error and adding to the semi-empirical model some additional weak newtonian damping, which is then used as a tuning parameter. It had turned out that both methods yield about the same results. Since the approach using the newtonian damping is less elaborate we have decided to pick this alternative for our present work.

each semi-empirical model by minimizing the *relative climate error*

$$\epsilon_c = \frac{1}{24} \sum_{m=1}^{12} (\epsilon_1^m + \epsilon_2^m) \,. \tag{15}$$

which is an average quantity calculated from the seasonally-dependent relative error of the first moments

$$\epsilon_1^m = \frac{\sum_{\nu=1}^{N} \left(\overline{a_\nu}^m_{model} - \overline{a_\nu}^m_{data}\right)^2}{\sum_{\nu=1}^{N} \left(\overline{a_\nu}^m_{data}\right)^2} \tag{16}$$

and the corresponding second-moment error

$$\epsilon_2^m = \frac{\sum_{\nu=1}^{N} \sum_{\mu=\nu}^{N} \left(\overline{a'_\nu a'_\mu}^m_{model} - \overline{a'_\nu a'_\mu}^m_{data}\right)^2}{\sum_{\nu=1}^{N} \sum_{\mu=\nu}^{N} \left(\overline{a'_\nu a'_\mu}^m_{data}\right)^2}. \tag{17}$$

The upper index m, running from 1 to 12, indicates the month for which the mean has been calculated. $a'_\nu(t) = a_\nu(t) - \overline{a_\nu}^m$ denotes transients.

3 The dynamical model core

From the previous discussion it is obvious that an essential part of a reduced semi-empirical model is the dynamical core. It should be energy-conserving in its discretized form, the conserved total energy should be a quadratic function of the prognostic variables, and the nonlinearities of the model should be of polynomial form. The filtered model used by AB satisfies all these criteria but for the reasons given above we have replaced it by some discretized version of the dry-adiabatic primitive equations. First a decision had to be made about the spatial discretization. It is important to note that one obvious candidate, viz. spectral primitive-equation models, violates total energy conservation due to the spectral truncation. We have therefore decided to use a longitude-latitude grid-point model along the ideas of Arakawa and Lamb (1977, 1981) and Takano and Wurtele (1982).

Furthermore, total energy in the primitive equation system is not really a positive definite quadratic function of the prognostic variables. If the vertical coordinate is $\sigma = p/p^s$ with p and p^s being pressure and surface pressure, respectively, then total energy is given by

$$E_{tot} = \frac{1}{g}\oint_A dA p^s \Phi^s + \frac{1}{g}\oint_V dV p^s \left(\frac{|\mathbf{V}|^2}{2} + c_p P\theta\right) \tag{18}$$

with $\oint_A dA = a^2 \int_0^{2\pi} d\lambda \int_{-\pi/2}^{\pi/2} d\phi \cos\phi$ and $\oint_V dV = a^2 \int_0^1 d\sigma \int_0^{2\pi} d\lambda \int_{-\pi/2}^{\pi/2} d\phi \cos\phi$ where a is the radius of the earth, λ and ϕ the geographical longitude and latitude, respectively, Φ^s the surface geopotential height, g the gravitational acceleration, $\mathbf{V}$ the horizontal wind, c_p the specific heat at constant pressure, θ the potential temperature, and $P = (p/p_0)^{R/c_p}$, with R being the gas constant for dry air, and p_0 some constant reference pressure. Obviously, the standard prognostic variables, surface pressure, horizontal wind, and potential temperature, cannot be used for our purposes. However, it is possible to reformulate and filter the equations such that potential temperature is replaced by its square root $\tau = \sqrt{\theta}$, and surface pressure is left time-independent.

Although the former replacement seems trivial, care must be taken to ensure that a numerical code using τ as temperature variable instead of θ still conserves energy. Neglecting the time-dependence of surface pressure is more fundamental since it eliminates the external Kelvin waves. This is a standard approach in oceanography (Bryan, 1969) where it is known as rigid-lid approximation. In the atmospheric context it has been used for pressure-coordinate models by Smagorinsky (1963) and Held and Suarez (1978). The consequence of this filter is nondivergence of the barotropic flow component $\langle\mathbf{V}\rangle = \int_0^1 d\sigma \mathbf{V}$, i.e. $\nabla \cdot p^s\langle\mathbf{V}\rangle = 0$. This follows from vertical integration of the continuity equation, with the appropriate boundary conditions ($\dot{\sigma} = 0$ at $\sigma = 0, 1$), and setting surface pressure time-independent. Consequently, there is a barotropic stream function

Ψ so that $p^s\langle\mathbf{V}\rangle = \mathbf{k}\times\nabla\Psi$, where $\mathbf{k}$ is the vertical unit vector. The real degrees of freedom of the horizontal flow are therefore provided by Ψ, and the baroclinic flow field $\hat{\mathbf{V}} = \mathbf{V} - \langle\mathbf{V}\rangle$ which has a vanishing vertical integral. As is readily shown, within this framework total energy can now be written as

$$E_f \;=\; \frac{1}{g}\oint_A dA\frac{|\nabla\Psi|^2}{2p^s} + \frac{1}{g}\oint_V dV p^s\left(\frac{\left|\hat{\mathbf{V}}\right|^2}{2} + c_p P\tau^2\right) \tag{19}$$

which is positive definite and quadratic in all variables, indeed.

The discretized form of the equations we have used is summarized in Appendix A. In extensive tests it has been verified that the introduction of time-independent surface pressure into the model with a resolution as specified below does not significantly affect the model dynamics: A benchmark test according to Held and Suarez (1994) was successful. Furthermore, in order to test the orographic impact which can be mediated to the model only via an orographically-conditioned surface pressure distribution, we have introduced for the latter its long-time mean from the coupled atmosphere/ocean GCM ECHAM3/LSG (Voss et al., 1998), and compared the model's behavior under solsticial zonally-symmetric heating to that of a standard primitive-equation code with external Kelvin waves and explicit orography. All mean states and transient fluxes turned out to be virtually the same.

4 The basis patterns: Global EOFs

As near-optimal basis patterns we have used global EOFs. Here and henceforth $\mathbf{X}$ shall be the state vector describing the dry state of the atmosphere, without time-dependent surface pressure, on a grid which is a staggered C-grid in the horizontal (Arakawa and Lamb, 1977) and uses σ-layers in the vertical. The metric is the total-energy metric corresponding to the filtered primitive equation model described in Appendix A, i.e. $E^{tot} = (\mathbf{X},\mathbf{X})$ is

the total energy conserved by the model equations. The constant surface pressure we have used is the same long-time mean from the GCM data as used in the benchmark test. The state space representation we have picked for the analysis transforms the energy metric to the identity matrix, thereby facilitating more straightforward calculations. For details the reader is referred to Appendix B.

The data set we have used consists of half-daily values for horizontal winds, temperature, and surface pressure from a 2000-year integration of the same coupled atmosphere/ocean general circulation model which we have taken the time-mean surface pressure from. They have been prepared by a linear interpolation from the model's 19 hybrid vertical levels to the $K_{lev} = 3$ layers at $\sigma = 0.833$, 0.5, and 0.167 and a consecutive bilinear interpolation to the staggered horizontal grid with $I_{lon} = 64$ longitudes and $J_{lat} = 32$ latitudes. The daily cycle has been removed by averaging between two consecutive states each. With the chosen resolution the matrix to be diagonalized is so large (16256^2 elements) that it could not be stored in the computer memory we had available. We have therefore resorted to an iterative approximate determination of the leading variance patterns, described in Appendix C. The analysis period was chosen such that when tested at the same number of independent data as were used for the pattern determination, the calculated EOFs were explaining nearly as much of the total variance as in the original data set. It was found that data from 100 years were sufficient.

Inspection of the time series of the corresponding principal components shows that the two leading EOFs are dominated by the strong seasonal cycle which explains about 30% of the total variance. Since we are interested also in a sufficient representation of the variance on top of the seasonal cycle the real quantity of interest is how many EOFs are needed for this. Figure 1 shows the relative variances which cannot be explained using a

given number of EOFs. The resulting numbers are quite similar to the ones obtained by AB from perpetual-january data: Nearly 500 EOFs are needed for explaining 90% of the variance on top of the seasonal cycle.

5 Estimation and analysis of the closure

The amount of data used for the tendency minimization (1140 years) was chosen such that it was well above the limit where a further significant increase does not change the model properties any more, with respect to both short term-prediction and climate simulation. In addition, the newtonian damping was determined as described above. For the calculation of the climate error in (15) the models have been integrated over periods of 100 years. The optimization of the constants A and β in (14) has been done with the help of a nonlinear simplex optimizer which chooses after each 100-year integration a new pair of parameters according to some selection rules ensuring convergence of the tuning process. The resulting parameters are summarized in table 1. The relaxation time of the additional damping of the first EOF is 178 days for the 10-EOF model, 4827 days for the 20-EOF model, and above 10000 days in all other cases, so that it is sufficiently small to ensure that, with the possible exception of the 10-EOF model, a correct reproduction of the seasonal cycle cannot be attributed to this extra term. It is also so small as not to affect the following analysis of the impact of the empirical parameterization on the model.

To begin with, solution of the linear regression problem yields tendency error minima for different numbers of basic EOFs as shown in figure 2. The corresponding errors for the projected models, and the relative errors determined by AB are also shown. Interestingly, already the projected three-layer primitive equation model performs better than the semi-empirical quasigeostrophic two-layer model. The parameterization scheme reduces the

errors further by a considerable amount so that we encounter tendency errors of less than 20% for the 500-EOF model. This seems to justify the effort we have put into the implementation of primitive-equation dynamics into reduced models since it makes their short-time behaviour much more similar to that of GCMs than before.

Some information about the geographical dependence of the tendency error can be extracted from figures 3-6. Figure 3 shows how the error in predicting tendencies of the barotropic streamfunction by the projected 500-EOF model depends on the horizontal location. Whereas this model performs quite well in the storm-track regions there is a conspicuous failure in the tropics and at the north pole. The inclusion of the empirical forcing terms (the zero-order part of the closure) reduces the errors in the tropics to about one third (Fig. 4). As shown in figure 5, the linear closure terms finally reduce the overall tendency errors so much that they are smaller than 30% in the tropics, and near 10% in midlatitudes. A qualitatively similar behaviour has also been observed for all other prognostic variables: The linear closure is of decisive importance for a good tendency prediction. Consequently also the total mean relative tendency error for all prognostic variables is 0.56 for the projected reduced model, 0.48 for the projected model with empirical forcing, and 0.18 for the complete semi-empirical model (including also the empirical linear terms). In spite of all progresses due to the incorporation of primitive-equation dynamics one should, however, also note that the semi-empirical model still performs best in midlatitudes. Problems in the tropical dynamics are most visible for the baroclinic flow field (cf., as an example, the layer-dependent relative tendency error for the zonal wind in figure 6) and for the thermodynamic variable (not shown).

We will not try to give dynamical interpretations of the empirical terms. The most prominent features of the 500-EOF closure shall, however, be described. Figure 7 shows

the zonal-mean empirical forcing of the meridional wind in January and July. Clearly, there is a tendency to enforce the winter-hemispheric Hadley circulation. Here one should recall that direct physical forcing components (heating due to radiation, convection, latent heat release etc.) appear only in the thermodynamic equation. So the fact that fixed empirical forcing terms appear in our momentum equations points at indirect forcing effects which may be understood as the net effect on the resolved components of nonlinear interactions among the unresolved components. Thus, although it is small in comparison to the leading order dynamical terms (by up to two orders of magnitude in comparison to the Coriolis term in the zonal-mean meridional-wind equation, not shown here), this direct forcing of the Hadley circulation points to an indirect effect which our low-order model can only handle in parameterized form. Figure 8 shows (for January) the zonal-mean empirical zonal-wind forcing and, for comparison, the time and zonal mean Coriolis term in the zonal-wind equation. Some indirect effects are parameterized, but especially in the tropics the forcing seems to be small by comparison. That our empirical approach can also yield forcing features one would expect from direct physical parameterizations can be seen in Figure 9, where the empirical forcing for the lower-level thermodynamic variable is shown. Obviously there is the typical heating pattern for lower-level air masses over land in the summer hemisphere, and the opposite pattern in the winter hemisphere.

As already deducible from the tendency errors shown above, the empirical linear terms are extremely important for getting the dynamics of the reduced model right. In fact, they are decisive for a correct description of the seasonal dependence of the dynamics of midlatitude synoptic eddies. For a visualization of this effect we have linearized our model, with and without empirical linear corrections, about the January or July mean state of the GCM. Following the standard procedure (e.g. Farrell and Ioannou, 1996) we have then

calculated from the resulting linear tensor the leading optimal vectors for 5-day lead time. What ought to be expected as result for a satisfactory model is a storm-track mode on the respective winter hemisphere. Indeed, the leading optimal vector of the semi-empirical model is a Pacific storm-track mode (Fig. 10), the following pattern reproduces it with a phase shift, and patterns 3 and 4 are corresponding northern-hemispheric Atlantic storm-track modes for January, and further southern-hemispheric Pacific storm-track modes for July (not shown). However, quite different structures result from calculations without empirical linear correction . As an example, figure 11 shows the obtained leading optimal vectors. They are quite different from those in figure 10, both in scale, in spatial extension, and in their location on the globe. This shows that the empirical linear terms are actually controlling the seasonally-dependent storm-track dynamics.

6 Summary and Discussion

In summary, our study represents a continuation of previous work on semi-empirical reduced models for the atmosphere. Generally, the development of such models is done in two main steps. In the first of those a near-optimal basis of EOFs is projected onto a dynamical model based on the fundamental geophysical fluid-dynamical equations (the dynamical core). The second step tries to make up for deficiencies of the thereby obtained projected model: Both the restriction to a low model dimension and a coarse resolution of the dynamical model core, e.g. in the vertical, necessarily lead to the neglect of the explicit treatment of certain small scales. The same holds for physical processes which are not explicitely described by the model (latent heat release, radiative transport, etc.). The important impact of these scales and processes is therefore parameterized by an empirical scheme which is extracted from some data set by minimization of the difference between

observed tendencies and the corresponding prediction of the reduced model. The models developed here differ from predecessors by two important modifications: For the first time the primitive equations have been used in the dynamical core, and a seasonal cycle has been incorporated.

The dynamical model core we have taken is a primitive-equation model which differs from its traditional counterparts by filtering external Kelvin waves. This enables the construction of a total energy metric consistent with the model, i.e. a metric with a norm which equals the total energy conserved by the discretized equations. Such a metric has two main advantages: First, using an EOF basis determined from the data with the help of this metric ensures that the projected model has no nonlinear instabilities which might otherwise lead to unbounded growth of energy. Secondly, in the data analysis the question arises as how to weight prognostic variables of different dynamical character (e.g. winds and temperature) with respect to each other. A natural solution to this question is provided by the use of an energy metric which weights each variable according to the energy variance associated to it. Technically, the filtering of external Kelvin waves is achieved by the use of a time-independent surface pressure, an approach which is parallel to the rigid-lid approximation used in oceanography. As a consequence the barotropic part of horizontal flow is nondivergent so that it must be described by an appropriate stream function. These ideas are implemented in a grid-point model which is described in the appendices.

Consequently, the basis patterns we have used are global EOFs describing simultaneously winds and temperature in all three spatial dimensions. They have been determined from atmosphere data of a 2000-year long run of a coupled ocean/atmosphere GCM (Voss et al., 1998). Since the overall state space is too large for being handled in a single co-

variance matrix the analysis has been done in an iterative way based on successive data compression in orthogonal subspaces. The variance analysis shows that, in spite of the presence of the seasonal cycle, the number of patterns necessary for explaining 90% of the variance on top of the seasonal cycle is about 500. This is an interesting number since it is in striking agreement with a previous result (Achatz and Branstator, 1999, in short AB) from an analysis of streamfunction data in two levels from a perpetual-january GCM dataset. It seems as if the atmosphere is not using different degrees of freedom for different seasons. Seasonality seems more to be brought about by a rearrangement of the respective relevance of the various circulation structures involved. This agrees with a corresponding result of Corti et al. (1999) on the mechanisms of climate change, encouraging us in our hope that EOF models might eventually be also useful for studies of climate variability.

The empirical closure we have used is of at most first order in the EOF-expansion coefficients. The empirical linear operator has as well a seasonal cycle as the zero-order terms, the external forcing. This turned out to be necessary for a correct simulation of the seasonal dependence in the fluxes due to transients. After the determination of the parameters of the scheme by tendency error minimization an additional damping was added. The damping coefficients were tuned by repeated 100-year integrations and minimization of the difference between the climate (first and second monthly moments) of the reduced model and the GCM.

As was to be expected, the primitive-equation model core enables the reduced semi-empirical models to predict instantaneous tendencies much better than previously used filtered equations. Without empirical parameterizations the relative tendency error is already considerably smaller than in the work of AB. Incorporation of the parameterization

reduces it to less than 20% if 500 EOFs are taken as basis. The corresponding reduction in tendency errors is global, but an especially pronounced effect can be seen in the tropics, indicating that much of the impact of small scales and physics there can be described linearly. Nonetheless, in the complete semi-empirical model the largest tendency errors are also still to be found in these regions, approaching 100% in some rare cases, so that plenty of room is left for further improvements by nonlinear physically-based parameterization schemes. The incorporation of moisture and explicit radiation might be interesting, as well as modern reduction techniques as e.g. described by Moise and Temam (2000). Finally, higher vertical resolution of the dynamical core could possibly also be important.

An analysis of how the empirical parameterization is achieving the tendency error reduction is most straightforwardly done for the empirical forcing. An investigation of the forcing fields showed some expected direct effects such as enhanced summer-time heating and winter-time cooling of lower air masses over the continents. In many cases, however, the forcing parameterizes some indirect physical or dynamical effects which are not explicitely described by the resolved model dynamics. As an example, at least part of the enhanced winter-hemispheric Hadley circulation is not brought about by seasonal variations in the heating patterns and consequential changes of the velocity field due to dynamical interactions, but by direct forcing of the meridional circulation. Similar conclusions can be drawn on the role of the empirical linear parameterization. An analysis of the equations, with and without these closure terms, for most rapidly growing structures in different seasons shows that the full semi-empirical model is very well predicting the expected storm track modes on the winter-hemisphere. This, however, is not the case for the model without empirical linear closure. Thus, it is the empirical linear terms which are effectively controlling the seasonality of storm-track dynamics.

Notwithstanding the overwhelming role the empirical part plays in the model, one should keep in mind that the successful incorporation of primitive-equation dynamics and seasonality into EOF-modelling seems to provide a more solid basis than ever before for research concerning low-frequency atmosphere dynamics with the help of low-order models. Further support for this view is provided in a companion paper which analyzes the climate simulated by our reduced models and reconsiders some old questions related to the dimensionality of the climate attractor and the origin of weather regimes.

Acknowledgements

The authors are indebted to R. Haarsma, F. Kwasniok, G. Schmitz, F. Selten, and A. Timmermann for numerous discussions helping us in different phases of the work. Furthermore we would like to acknowledge the helpful comments of C. Penland and two anonymous reviewers which have lead to substantial improvements in the manuscript. Special thanks are due to R. Voss for allowing us to use his GCM data. The enormous help of X. Wang in retreiving those data from the archives is also gratefully acknowledged. A major part of the research has been done while U.A. was a visiting scientist at KNMI.

Appendix A A grid-point model for the primitive equations without external Kelvin waves

Appendix A.1 Introduction of a new thermodynamic variable

Introducing $\tau = \sqrt{\theta}$ the continuous primitive equations to be discretized (e.g. Arakawa and Lamb, 1977, 1981) can be written in spherical coordinates

$$\frac{\partial}{\partial t}\frac{u}{m} - q\frac{vp^s}{m} + \frac{\partial}{\partial \lambda}\left(\frac{u^2+v^2}{2} + \Phi\right) + \alpha_v \sigma \frac{\partial p^s}{\partial \lambda} + \frac{\dot{\sigma}}{m}\frac{\partial u}{\partial \sigma} = \frac{F_\lambda}{m} \tag{A1}$$

$$\frac{\partial}{\partial t}\frac{v}{n} + q\frac{up^s}{n} + \frac{\partial}{\partial \phi}\left(\frac{u^2+v^2}{2} + \Phi\right) + \alpha_v \sigma \frac{\partial p^s}{\partial \phi} + \frac{\dot{\sigma}}{n}\frac{\partial v}{\partial \sigma} = \frac{F_\phi}{n} \tag{A2}$$

$$\delta\left(\Phi\sigma\right) + \left(p^s \sigma \alpha_v - \Phi\right)\delta\sigma = 0 \tag{A3}$$

$$\frac{\partial}{\partial t}\frac{p^s}{mn} + \frac{\partial}{\partial \lambda}\frac{p^s u}{n} + \frac{\partial}{\partial \phi}\frac{p^s v}{m} + \frac{\partial}{\partial \sigma}\frac{p^s \dot{\sigma}}{mn} = 0 \tag{A4}$$

$$\frac{\partial}{\partial t}\frac{\tau p^s}{mn} + \frac{\partial}{\partial \lambda}\frac{p^s u}{n}\tau + \frac{\partial}{\partial \phi}\frac{p^s v}{m}\tau + \frac{\partial}{\partial \sigma}\frac{p^s \dot{\sigma}}{mn}\tau = \frac{p^s Q}{2\tau c_p P n m} \tag{A5}$$

where u and v are respectively the zonal and meridional velocity, and the metric factors are $m = 1/(a\cos\phi)$ and $n = 1/a$. Furthermore, f is the Coriolis parameter, ζ the relative vorticity, and $q = (f+\zeta)/p^s$. Φ is the geopotential height, α_v the specific volume, $\mathbf{F}$ denotes friction, and Q heating.

The horizontal discretization is done on a staggered Arakawa-C-grid with longitude and latitude indices i and j, counting eastwards from 1 to I_{lon} and northwards from 1 to J_{lat}. For details of the grid specification the reader is refered to Arakawa and Lamb (1981). The vertical grid is also staggered with a corresponding index k counting from 1 to K_{lev}. The distribution of variables is as in Arakawa and Lamb (1977). Our notation differs from there by using half-levels for σ and its time derivative, and full levels for all other fields, instead of even and odd levels. The discretized equations given below are written so as to conserve total energy as well as total mass, the global integrals of $p^s\tau$

and $p^s\theta = p^s\tau^2$, and in the shallow water limit also potential enstrophy. For conciceness we introduce the following shortcuts for longitudinal differencing, linear averaging, and arithmetic averaging of some quantity X:

$$\left(\delta_\lambda X\right)_{i,\cdot} = X_{i+\frac{1}{2},\cdot} - X_{i-\frac{1}{2},\cdot} \tag{A6}$$

$$\left(\overline{X}^\lambda\right)_{i,\cdot} = \frac{1}{2}\left(X_{i+\frac{1}{2},\cdot} + X_{i-\frac{1}{2},\cdot}\right) \tag{A7}$$

$$\left(\widetilde{X^2}^\lambda\right)_{i+\frac{1}{2},\cdot} = X_{i,\cdot}X_{i+1,\cdot}. \tag{A8}$$

Analogous notation holds for the corresponding latitudinal and vertical operations. For the area differential we write $\Delta A = (\Delta\lambda\Delta\phi)/(mn)$. It should be noted that the longitude differential $\Delta\lambda$ is constant whereas the latitude differential $\Delta\phi$ depends on the latitude. Let us now also define the local product of surface pressure and area differential

$$P^s_{i+\frac{1}{2},j+\frac{1}{2}} = \left(\Delta A p^s\right)_{i+\frac{1}{2},j+\frac{1}{2}} \tag{A9}$$

so that shallow-water potential vorticity becomes

$$q_{i,j,k} = 4\frac{\left[\Delta A\left(f+\zeta\right)\right]_{i,j,k}}{P^s_{i+\frac{1}{2},j+\frac{1}{2}} + P^s_{i-\frac{1}{2},j+\frac{1}{2}} + P^s_{i+\frac{1}{2},j-\frac{1}{2}} + P^s_{i-\frac{1}{2},j-\frac{1}{2}}} \tag{A10}$$

where relative vorticity is calculated via

$$\zeta_{i,j,k} = \frac{1}{\Delta A_{i,j}}\left(\delta_\lambda\frac{v\Delta\phi}{n} - \delta_\phi\frac{u\Delta\lambda}{m}\right)_{i,j,k}. \tag{A11}$$

ζ and q at the poles are obtained from

$$q_{i,J_{lat},k} = \frac{\left(f+\zeta\right)_{i,J_{lat},k}}{\left(\sum_{i=1}^{I_{lon}} p^s_{i,J_{lat}-\frac{1}{2}}\right)/I_{lon}} \tag{A12}$$

$$q_{i,1,k} = \frac{\left(f+\zeta\right)_{i,1,k}}{\left(\sum_{i=1}^{I_{lon}} p^s_{i,\frac{3}{2}}\right)/I_{lon}} \tag{A13}$$

$$\zeta_{i,J_{lat},k} = \frac{1}{\Delta A_n}\sum_{i=1}^{I_{lon}}\left(\frac{u\Delta\lambda}{m}\right)_{i,J_{lat}-\frac{1}{2},k} \tag{A14}$$

$$\zeta_{i,1,k} = -\frac{1}{\Delta A_s}\sum_{i=1}^{I_{lon}}\left(\frac{u\Delta\lambda}{m}\right)_{i,\frac{3}{2},k} \tag{A15}$$

with $\Delta A_n = \frac{I_{lon}}{2}(\Delta A)_{J_{lat}-\frac{1}{2}}$ and $\Delta A_s = \frac{I_{lon}}{2}(\Delta A)_{\frac{3}{2}}$. Furthermore we introduce the velocity related quantities

$$u^*_{i,j+\frac{1}{2},k} = \left(\overline{p^s}^{\lambda} u \frac{\Delta\phi}{n}\right)_{i,j+\frac{1}{2},k} \tag{A16}$$

and

$$v^*_{i+\frac{1}{2},j,k} = \left(\overline{p^s}^{\phi} v \frac{\Delta\lambda}{m}\right)_{i+\frac{1}{2},j,k} \tag{A17}$$

With these definitions the fourth-order accurate analogues of the terms $A^u = -q(vp^s/m)$ and $A^v = q(up^s/n)$ in the momentum equations become (Takano and Wurtele, 1982)

$$\begin{aligned}
A^u(\mathbf{V},q)_{i,j+\frac{1}{2},k} &= -\alpha_{i,j+\frac{1}{2},k} v^*_{i+\frac{1}{2},j+1,k} - \beta_{i,j+\frac{1}{2},k} v^*_{i-\frac{1}{2},j+1,k} \\
&\quad -\gamma_{i,j+\frac{1}{2},k} v^*_{i-\frac{1}{2},j,k} - \delta_{i,j+\frac{1}{2},k} v^*_{i+\frac{1}{2},j,k} \\
&\quad +\epsilon_{i+\frac{1}{2},j+\frac{1}{2},k} u^*_{i+1,j+\frac{1}{2},k} - \epsilon_{i-\frac{1}{2},j+\frac{1}{2},k} u^*_{i-1,j+\frac{1}{2},k} \\
&\quad +\lambda_{i,j+1,k} u^*_{i,j+\frac{3}{2},k} - \lambda_{i,j,k} u^*_{i,j-\frac{1}{2},k}
\end{aligned} \tag{A18}$$

$$\begin{aligned}
A^v(\mathbf{V},q)_{i+\frac{1}{2},j,k} &= \gamma_{i+1,j+\frac{1}{2},k} u^*_{i+1,j+\frac{1}{2},k} + \delta_{i,j+\frac{1}{2},k} u^*_{i,j+\frac{1}{2},k} \\
&\quad +\alpha_{i,j-\frac{1}{2},k} u^*_{i,j-\frac{1}{2},k} + \beta_{i+1,j-\frac{1}{2},k} u^*_{i+1,j-\frac{1}{2},k} \\
&\quad +\psi_{i+\frac{1}{2},j+\frac{1}{2},k} v^*_{i+\frac{1}{2},j+1,k} - \psi_{i+\frac{1}{2},j-\frac{1}{2},k} v^*_{i+\frac{1}{2},j-1,k} \\
&\quad +\mu_{i+1,j,k} v^*_{i+\frac{3}{2},j,k} - \mu_{i,j,k} v^*_{i-\frac{1}{2},j,k}.
\end{aligned} \tag{A19}$$

Here the contributing coefficients are

$$\begin{aligned}
\alpha_{i,j+\frac{1}{2},k} &= \frac{1}{24}(2q_{i+1,j+1,k} + 3q_{i,j+1,k} + 2q_{i,j,k} + q_{i+1,j,k} - q_{i,j+2,k} - q_{i-1,j+1,k}) \\
\beta_{i,j+\frac{1}{2},k} &= \frac{1}{24}(3q_{i,j+1,k} + 2q_{i-1,j+1,k} + q_{i-1,j,k} + 2q_{i,j,k} - q_{i+1,j+1,k} - q_{i,j+2,k}) \\
\gamma_{i,j+\frac{1}{2},k} &= \frac{1}{24}(2q_{i,j+1,k} + q_{i-1,j+1,k} + 2q_{i-1,j,k} + 3q_{i,j,k} - q_{i,j-1,k} - q_{i+1,j,k}) \\
\delta_{i,j+\frac{1}{2},k} &= \frac{1}{24}(q_{i+1,j+1,k} + 2q_{i,j+1,k} + 3q_{i,j,k} + 2q_{i+1,j,k} - q_{i-1,j,k} - q_{i,j-1,k}) \\
\epsilon_{i+\frac{1}{2},j+\frac{1}{2},k} &= \frac{1}{24}(q_{i+1,j+1,k} + q_{i,j+1,k} - q_{i,j,k} - q_{i+1,j,k})
\end{aligned}$$

$$\begin{aligned}
\psi_{i+\frac{1}{2},j+\frac{1}{2},k} &= \frac{1}{24}\left(-q_{i+1,j+1,k}+q_{i,j+1,k}+q_{i,j,k}-q_{i+1,j,k}\right)\\
\lambda_{i,j,k} &= \frac{1}{24}\left(q_{i+1,j,k}-q_{i-1,j,k}\right)\\
\mu_{i,j,k} &= \frac{1}{24}\left(q_{i,j-1,k}-q_{i,j+1,k}\right).
\end{aligned} \tag{A20}$$

Finally one needs kinetic energy at scalar points

$$K_{i+\frac{1}{2},j+\frac{1}{2},k}=\frac{1}{2\Delta A_{i+\frac{1}{2},j+\frac{1}{2}}}\left(\overline{\Delta A u^2}^{\lambda}+\overline{\Delta A v^2}^{\phi}\right)_{i+\frac{1}{2},j+\frac{1}{2},k} \tag{A21}$$

and the σ-velocities above and below horizontal-velocity points

$$\dot{\sigma}^{u}_{i,j+\frac{1}{2},k+\frac{1}{2}} = \left(\frac{\overline{p^s\dot{\sigma}}^{\lambda}}{\overline{p^s}^{\lambda}}\frac{\Delta\lambda}{m}\right)_{i,j+\frac{1}{2},k+\frac{1}{2}} \tag{A22}$$

$$\dot{\sigma}^{v}_{i+\frac{1}{2},j,k+\frac{1}{2}} = \left(\frac{\overline{p^s\dot{\sigma}}^{\phi}}{\overline{p^s}^{\phi}}\frac{\Delta\phi}{n}\right)_{i+\frac{1}{2},j,k+\frac{1}{2}}. \tag{A23}$$

The latter enter the vertical momentum advection terms via

$$\left(\dot{\sigma}^{X}\frac{\partial X}{\partial\sigma}\right)_{\cdot,k}=\frac{1}{2\Delta\sigma_k}\left[\left(X_{\cdot,k+1}-X_{\cdot,k}\right)\dot{\sigma}^{X}_{\cdot,k+\frac{1}{2}}+\left(X_{\cdot,k}-X_{\cdot,k-1}\right)\dot{\sigma}^{X}_{\cdot,k-\frac{1}{2}}\right] \tag{A24}$$

where X is either u or v, and $\Delta\sigma_k=\sigma_{k+\frac{1}{2}}-\sigma_{k-\frac{1}{2}}$. With all the definitions given above the discretized momentum equations are now

$$\left[\frac{\Delta\lambda}{m}\frac{\partial u}{\partial t}+A^u\left(\mathbf{V},q\right)+\delta_\lambda\left(K+\Phi\right)+\sigma\alpha_v\delta_\lambda p^s+\dot{\sigma}^u\frac{\partial u}{\partial\sigma}\right]_{i,j+\frac{1}{2},k} = \left(\frac{F_\lambda}{m}\Delta\lambda\right)_{i,j+\frac{1}{2},k} \tag{A25}$$

$$\left[\frac{\Delta\phi}{n}\frac{\partial v}{\partial t}+A^v\left(\mathbf{V},q\right)+\delta_\phi\left(K+\Phi\right)+\sigma\alpha_v\delta_\phi p^s+\dot{\sigma}^v\frac{\partial v}{\partial\sigma}\right]_{i+\frac{1}{2},j,k} = \left(\frac{F_\phi}{n}\Delta\phi\right)_{i+\frac{1}{2},j,k} \tag{A26}$$

The continuity equation becomes

$$\left(\frac{\partial P^s}{\partial t}+\delta_\lambda u^*+\delta_\phi v^*+P^s\frac{\delta_\sigma\dot{\sigma}}{\Delta\sigma}\right)_{i+\frac{1}{2},j+\frac{1}{2},k}=0. \tag{A27}$$

Discretization of the first law of thermodynamics is done via

$$\left[\frac{\partial}{\partial t}\left(\tau P^s\right)+\delta_\lambda\left(u^*\overline{\tau}^{\lambda}\right)+\delta_\phi\left(v^*\overline{\tau}^{\phi}\right)+P^s\frac{\delta_\sigma\left(\dot{\sigma}\tau\right)}{\Delta\sigma}\right]_{i+\frac{1}{2},j+\frac{1}{2},k} = \left(\frac{P^sQ}{2\tau c_pP}\right)_{i+\frac{1}{2},j+\frac{1}{2},k} \tag{A28}$$

with

$$\tau_{i+\frac{1}{2},j+\frac{1}{2},k+\frac{1}{2}} = \frac{1}{2}\left(\tau_{i+\frac{1}{2},j+\frac{1}{2},k} + \tau_{i+\frac{1}{2},j+\frac{1}{2},k+1}\right). \tag{A29}$$

(A25) and (A26) need the specific volume at u- and v-points, given by

$$(\sigma\alpha_v)_{i,j+\frac{1}{2},k} = c_p\left(\widetilde{\tau^2}^{\lambda}\frac{\delta_\lambda P}{\delta_\lambda p^s}\right)_{i,j+\frac{1}{2},k} \tag{A30}$$

$$(\sigma\alpha_v)_{i+\frac{1}{2},j,k} = c_p\left(\widetilde{\tau^2}^{\phi}\frac{\delta_\phi P}{\delta_\phi p^s}\right)_{i+\frac{1}{2},j,k} \tag{A31}$$

The hydrostatic equation is solved using

$$\Phi_{i+\frac{1}{2},j+\frac{1}{2},k} = \Phi_{i+\frac{1}{2},j+\frac{1}{2},k+1} + c_p\left(\widetilde{\tau^2}^{\sigma}\delta_\sigma P\right)_{i+\frac{1}{2},j+\frac{1}{2},k+\frac{1}{2}}. \tag{A32}$$

and

$$\begin{aligned}\Phi_{i+\frac{1}{2},j+\frac{1}{2},K_{lev}} &= \Phi^s_{i+\frac{1}{2},j+\frac{1}{2}} + c_p p^s_{i+\frac{1}{2},j+\frac{1}{2}}\sum_{k=1}^{K_{lev}}\Delta\sigma_k\left(\tau^2\frac{\partial P}{\partial p^s}\right)_{i+\frac{1}{2},j+\frac{1}{2},k}\\ &\quad -c_p\sum_{k=1}^{K_{lev}-1}\sigma_{k+\frac{1}{2}}\left(\widetilde{\tau^2}^{\sigma}\delta_\sigma P\right)_{i+\frac{1}{2},j+\frac{1}{2},k+\frac{1}{2}}.\end{aligned} \tag{A33}$$

What is still lacking is a recipe for calculating P at full levels. With this respect we follow Arakawa and Lamb (1977) by using

$$P_{i+\frac{1}{2},j+\frac{1}{2},k} = \left(\frac{p^s_{i+\frac{1}{2},j+\frac{1}{2}}}{p_0}\right)^{R/c_p}\left(\frac{1}{1+a}\frac{\sigma^{1+a}_{k+\frac{1}{2}}-\sigma^{1+a}_{k-\frac{1}{2}}}{\sigma_{k+\frac{1}{2}}-\sigma_{k-\frac{1}{2}}}\right)^{\frac{R}{c_p a}} \tag{A34}$$

with $a = 0.205$.

Appendix A.2 Filtering of external Kelvin waves

As sketched in section 3 we will now remove all nonlinearities from the model which are of higher order than quadratic, and also make the conserved energy positive definite and quadratic in the model variables, by setting the surface pressure time independent. The continuity equation then becomes

$$\left(\delta_\lambda u^* + \delta_\phi v^* + P^s\frac{\delta_\sigma\dot{\sigma}}{\Delta\sigma}\right)_{i+\frac{1}{2},j+\frac{1}{2},k} = 0 \tag{A35}$$

which yields, after multiplying by $\Delta\sigma_k$ and taking the sum over all levels,

$$(\delta_\lambda \langle u^* \rangle + \delta_\phi \langle v^* \rangle)_{i+\frac{1}{2},j+\frac{1}{2},k} = 0 \tag{A36}$$

where we have used the notation $\langle X \rangle_\cdot = \sum_{k=1}^{K_{lev}} \Delta\sigma_k X_{\cdot,k}$ for the vertical average of an arbitrary quantity X. This nondivergence of the vertically averaged flow implies, as in the continuous case, the existence of a barotropic streamfunction $\Psi_{i,j}$ so that

$$\langle u^* \rangle_{i,j+\frac{1}{2}} = -(\delta_\phi \Psi)_{i,j+\frac{1}{2}} \tag{A37}$$

$$\langle v^* \rangle_{i+\frac{1}{2},j} = (\delta_\lambda \Psi)_{i+\frac{1}{2},j}\,. \tag{A38}$$

Given a boundary value of Ψ at one of the poles (we have set $\Psi_{\cdot,J_{lat}} = 0$) it can be determined through these relations from the barotropic flow field. A more practical way is to first calculate relative barotropic vorticity via

$$\langle \zeta \rangle_{i,j} = \frac{1}{\Delta A_{i,j}} \left(\delta_\lambda \frac{\langle v \rangle \Delta\phi}{n} - \delta_\phi \frac{\langle u \rangle \Delta\lambda}{m} \right)_{i,j} \tag{A39}$$

and the corresponding relation for the south pole, to be obtained from (A15). The barotropic streamfunction can then be determined from

$$(\Delta A \langle \zeta \rangle)_{i,j} = (\mathsf{V}\Psi)_{i,j} \tag{A40}$$

where V is the vorticity operator, the discretized analogue of $\nabla \cdot \frac{\nabla}{p^s}$, whose elements can be obtained from (A39) and its counterpart for the south pole, (A16), (A17), (A37), and (A38). Finally, let us also introduce the baroclinic velocities $\hat{u}$ and $\hat{v}$. For any quantity X we define $\hat{X} = X - \langle X \rangle$. Since $\langle \hat{X} \rangle = 0$ the value of $\hat{X}$ on one layer is not independent but must be calculated from the other ones. For consistency we now replace u and v as prognostic variables by Ψ and the values of $\hat{u}$ and $\hat{v}$ on all levels but the lowest one. Their tendencies can be obtained from $\partial u/\partial t$ and $\partial v/\partial t$ in (A25) and (A26) by calculating first

the time derivative of relative barotropic vorticity from

$$\left(\frac{\partial\langle\zeta\rangle}{\partial t}\right)_{i,j} = \frac{1}{\Delta A_{i,j}}\left(\delta_\lambda \frac{\langle\frac{\partial v}{\partial t}\rangle\Delta\phi}{n} - \delta_\phi \frac{\langle\frac{\partial u}{\partial t}\rangle\Delta\lambda}{m}\right)_{i,j} \tag{A41}$$

and the corresponding relation at the south pole,

$$\left(\frac{\partial\langle\zeta\rangle}{\partial t}\right)_{i,1} = -\frac{1}{\Delta A_s}\sum_{i=1}^{I_{lon}}\left(\frac{\langle\frac{\partial u}{\partial t}\rangle\Delta\lambda}{m}\right)_{i,\frac{3}{2}}, \tag{A42}$$

and then determining the barotropic streamfunction tendencies from the time derivative of (A40). Additionally,

$$\left(\frac{\partial\hat{u}}{\partial t}\right)_{i,j+\frac{1}{2},k} = \left(\frac{\partial u}{\partial t} - \langle\frac{\partial u}{\partial t}\rangle\right)_{i,j+\frac{1}{2},k} \tag{A43}$$

$$\left(\frac{\partial\hat{v}}{\partial t}\right)_{i+\frac{1}{2},j,k} = \left(\frac{\partial v}{\partial t} - \langle\frac{\partial v}{\partial t}\rangle\right)_{i+\frac{1}{2},j,k} \tag{A44}$$

yield the tendencies of the baroclinic velocities. Finally, the hydrostatic equation and the first law of thermodynamics stay as in the unfiltered model. A difference is that the surface geopotential height does not appear in the final dynamic equations since its horizontal gradient is irrotational and independent of the vertical coordinate. The orographic impact is mediated indirectly to the model by the surface pressure distribution which mirrors the surface height variations over the globe. Using some algebra one can check that the continuous model actually conserves total energy E_f as given in (19), and that the discretized equations conserve its analogue $E_f = E^{kin}_{btp} + E^{kin}_{bcl} + E^{th}$ where the barotropic and baroclinic parts of kinetic energy are respectively

$$E^{kin}_{btp} = \frac{1}{g}\sum_{i=1}^{I_{lon}}\left\{\sum_{j=2}^{J_{lat}-1}\left[\frac{m\Delta\phi}{n\Delta\lambda}\frac{(\delta_\lambda\Psi)^2}{2\overline{p^s}^\phi}\right]_{i+\frac{1}{2},j} + \sum_{j=1}^{J_{lat}-1}\left[\frac{n\Delta\lambda}{m\Delta\phi}\frac{(\delta_\phi\Psi)^2}{2\overline{p^s}^\lambda}\right]_{i,j+\frac{1}{2}}\right\} \tag{A45}$$

$$E^{kin}_{bcl} = \frac{1}{g}\sum_{i=1}^{I_{lon}}\sum_{k=1}^{K_{lev}}\Delta\sigma_k\left[\sum_{j=1}^{J_{lat}-1}\left(\Delta A\overline{p^s}^\lambda\frac{\hat{u}^2}{2}\right)_{i,j+\frac{1}{2},k} + \sum_{j=2}^{J_{lat}-1}\left(\Delta A\overline{p^s}^\phi\frac{\hat{v}^2}{2}\right)_{i+\frac{1}{2},j,k}\right] \tag{A46}$$

and total enthalpy is given by

$$E^{th} = \frac{1}{g}\sum_{i=1}^{I_{lon}}\sum_{j=1}^{J_{lat}-1}\sum_{k=1}^{K_{lev}}\Delta\sigma_k c_p\left(P^s P\tau^2\right)_{i+\frac{1}{2},j+\frac{1}{2},k} \tag{A47}$$

Appendix B Diagonalization of the energy metric

For practical applications, e.g. the EOF-determination, it is useful to introduce model variables which render the energy metric diagonal. In fact these can even be associated with some dynamical meaning which may be seen from the following: Applying the differencing rules (holding for arbitrary quantities X and Y, ρ being either λ or ϕ)

$$\delta_\rho \left(X \overline{Y}^\rho \right) = Y \delta_\rho X + \overline{X \delta_\rho Y}^\rho \tag{B1}$$

to the baroptropic part of total energy one finds

$$\begin{aligned} E_{btp}^{kin} &= -\frac{1}{2g} \sum_{i=1}^{I_{lon}} \sum_{j=1}^{J_{lat}-1} \left\{ \Psi \left[\delta_\lambda \left(\frac{m \Delta\phi}{n \Delta\lambda} \frac{\delta_\lambda \Psi}{\overline{p^s}^\phi} \right) + \delta_\phi \left(\frac{n \Delta\lambda}{m \Delta\phi} \frac{\delta_\phi \Psi}{\overline{p^s}^\lambda} \right) \right] \right\}_{i,j} \\ &= -\mathbf{\Psi}^t \frac{\mathsf{V}}{2g} \mathbf{\Psi} \end{aligned} \tag{B2}$$

where we have gathered all $N_{btp} = I_{lon}(J_{lat} - 2)$ independent grid-point values of the barotropic streamfunction in a vector $\mathbf{\Psi}$. Furthermore we use the convention that $(\delta_\phi \Psi)_{i,\frac{1}{2}} = 0$. V is the barotropic vorticity operator. It is easily checked that it is symmetric and therefore has orthogonal eigenvectors which reduce in the limit of spatially constant surface pressure to discretized analogues of the spherical harmonics. Denoting these by $\mathbf{\Psi}^\nu$ we obtain

$$E_{btp}^{kin} = \sum_{\nu=1}^{N_{btp}} \tilde{\Psi}_\nu^2 \tag{B3}$$

where

$$\mathbf{\Psi} = \sum_{\nu=1}^{N_{btp}} \tilde{\Psi}_\nu \mathbf{\Psi}^\nu, \tag{B4}$$

and the eigenvectors have been normalized so that

$$\mathbf{\Psi}^{\nu t} \mathbf{\Psi}^\nu = -\frac{2g}{\lambda_\nu} \tag{B5}$$

with λ_ν being the corresponding eigenvalue. Furthermore, due to the vanishing vertical integral of $\hat{u}$ and $\hat{v}$ we have for the baroclinic part of kinetic energy

$$\begin{aligned} E_{bcl}^{kin} &= \frac{1}{g}\sum_{i=1}^{I_{lon}}\sum_{k=1}^{K_{lev}}\Delta\sigma_k\left[\sum_{j=1}^{J_{lat}-1}\left(\Delta A\overline{p^s}^{\lambda}\frac{\hat{u}^2}{2}\right)_{i,j+\frac{1}{2},k}+\sum_{j=2}^{J_{lat}-1}\left(\Delta A\overline{p^s}^{\phi}\frac{\hat{v}^2}{2}\right)_{i+\frac{1}{2},j,k}\right] \\ &= \frac{1}{2g}\sum_{i=1}^{I_{lon}}\left[\sum_{j=1}^{J_{lat}-1}\left(\Delta A\overline{p^s}^{\lambda}\right)_{i,j+\frac{1}{2}}\sum_{k=1}^{K_{lev}-1}\sum_{l=1}^{K_{lev}-1}\hat{u}_{i,j+\frac{1}{2},k}M_{kl}^{bcl}\hat{u}_{i,j+\frac{1}{2},l}\right. \\ &\quad \left.+\sum_{j=2}^{J_{lat}-1}\left(\Delta A\overline{p^s}^{\phi}\right)_{i+\frac{1}{2},j}\sum_{k=1}^{K_{lev}-1}\sum_{l=1}^{K_{lev}-1}\hat{v}_{i+\frac{1}{2},j,k}M_{kl}^{bcl}\hat{v}_{i+\frac{1}{2},j,l}\right] \end{aligned} \tag{B6}$$

The matrix

$$M_{kl}^{bcl}=\delta_{kl}\Delta\sigma_k+\frac{\Delta\sigma_k\Delta\sigma_l}{\Delta\sigma_{K_{lev}}} \tag{B7}$$

is again symmetric and therefore has orthogonal $(K_{lev}-1)$-dimensional eigenvectors. Denoting the corresponding eigenvalues by μ_k we choose their normalization to depend on the horizontal location and whether we are dealing with zonal or meridional velocities:

$$\left(\hat{\mathbf{u}}_{\mathbf{i},\mathbf{j}+\frac{1}{2}}^{\mathbf{k}}\right)^t\hat{\mathbf{u}}_{\mathbf{i},\mathbf{j}+\frac{1}{2}}^{\mathbf{k}}=\frac{2g}{\mu_k\left(\Delta A\overline{p^s}^{\lambda}\right)_{i,j+\frac{1}{2}}} \tag{B8}$$

$$\left(\hat{\mathbf{v}}_{\mathbf{i}+\frac{1}{2},\mathbf{j}}^{\mathbf{k}}\right)^t\hat{\mathbf{v}}_{\mathbf{i}+\frac{1}{2},\mathbf{j}}^{\mathbf{k}}=\frac{2g}{\mu_k\left(\Delta A\overline{p^s}^{\phi}\right)_{i+\frac{1}{2},j}}. \tag{B9}$$

Then we get

$$E_{bcl}^{kin}=\sum_{k=1}^{K_{lev}-1}\sum_{i=1}^{I_{lon}}\left[\sum_{j=1}^{J_{lat}-1}\tilde{u}_{i,j+\frac{1}{2},k}^2+\sum_{j=2}^{J_{lat}-1}\tilde{v}_{i+\frac{1}{2},j,k}^2\right] \tag{B10}$$

where

$$\hat{u}_{i,j+\frac{1}{2},k} = \sum_{l=1}^{K_{lev}-1}\tilde{u}_{i,j+\frac{1}{2},l}\hat{u}_{i,j+\frac{1}{2},k}^{l} \tag{B11}$$

$$\hat{v}_{i+\frac{1}{2},j,k} = \sum_{l=1}^{K_{lev}-1}\tilde{v}_{i+\frac{1}{2},j,l}\hat{v}_{i+\frac{1}{2},j,k}^{l}. \tag{B12}$$

Finally we also introduce the rescaled thermodynamic variable

$$\tilde{\tau}_{i+\frac{1}{2},j+\frac{1}{2},k}=\tau_{i+\frac{1}{2},j+\frac{1}{2},k}\sqrt{\frac{\Delta\sigma_k c_p\left(P^sP\right)_{i+\frac{1}{2},j+\frac{1}{2},k}}{g}} \tag{B13}$$

so that the energy metric with respect to the new variables $\tilde{\Psi}$, $\tilde{u}$, $\tilde{v}$, and $\tilde{\tau}$ is of the simple euclidian type.

Appendix C Iterative EOF-determination

Our EOF analysis relies on successive data compression using non-global preliminary EOFs: After calculation of the long-time mean state of the data we have determined in a first step seperate horizontal EOFs for the barotropic streamfunction coefficients, either the total horizontal field of baroclinic zonal wind or baroclinic meridional wind projecting on each of the $K_{lev} - 1$ vertical baroclinic energy-metric eigenvectors (see Appendix B), and the thermodynamic variable in each layer. In a second step the baroclinic zonal-wind fields were combined by picking for the horizontal subspaces projecting on each of the latter baroclinic eigenvectors enough EOFs so as to explain 99.9% of the respective total variance. By projecting onto these patterns a compressed representation of the total baroclinic zonal-wind field was achieved in which a simualtaneous analysis of the three-dimensional field was possible, yielding corresponding new EOFs. The same procedure was repeated for combining the horizontal subspaces projecting on each of the baroclinic eigenvectors for the meridional wind field, and for a combined analysis of the thermodynamic variable on all layers. Thus we had four sets of EOFs, one for the barotropic streamfunction, one for the baroclinic zonal wind, one for the baroclinic meridional wind, and one for the thermodynamic variable on all layers. From each of these sets we have then picked in a third analysis step enough EOFs as necessary for explaining again 99.9%, respectively. Projecting onto these we could obtain a data compression which left the remaining state vector small enough for a simultaneous analysis of all variables.

References

Achatz, U., and G. Schmitz, 1997: On the closure problem in the reduction of complex atmospheric models by PIPs and EOFs: A comparison for the case of a two-layer model with zonally symmetric forcing. *J. Atmos. Sci.*, **54**, 2452-2474

Achatz, U., and G. Branstator, 1999: A two-layer model with empirical linear corrections and reduced order for studies of internal climate variability. *J. Atmos. Sci.*, **56**, 3140-3160

Arakawa, A., and V. R. Lamb, 1977: Computational design of the basic dynamical processes of the UCLA general circulation model, *Methods in Computational Physics*, **17**, 173-265

Arakawa, A., and V. R. Lamb, 1981: A potential enstrophy and energy conserving scheme for the shallow water equations. *Mon. Wea. Rev.*, **109**, 18-36

Bryan, K., 1969: A numerical method for the study of the circulation of the world ocean. *J. Computational Phys.*, **4**, 347-376

Charney, J., and J.G. DeVore, 1979: Multiple flow equilibria in the atmosphere and blocking. *J. Atmos. Sci.*, **36**, 1205-1216

Corti, S., F. Molteni, and T.N. Palmer, 1999: Signature of recent climate change in frequencies of natural atmospheric circulation regimes. *Nature*, **398**, 799-802

d'Andrea, F., and R. Vautard, 2001: Extratropical low-frequency variability as a low-dimensional problem. I: A simplified model. *Quart. J. Roy. Meteor. Soc.*, **127**, 1357-1374

DelSole, T., 1996: Can quasigeostrophic turbulence be modeled stochastically? *J. Atmos. Sci.*, **53**, 1617-1633

DelSole, T., and A.Y. Hou, 1999: Empirical stochastic models for the dominant climate statistics of a general circulation model. *J. Atmos. Sci.*, **56**, 3436-3456

DelSole, T., 2001: A theory for the forcing and dissipation in stochastic turbulence models. *J. Atmos. Sci.*, **58**, 3762-3775

Farrell, B.F., and P.J. Ioannou, 1993: Stochastic dynamics of baroclinic waves. *J. Atmos. Sci.*, **50**, 4044-4057

Farrell, B.F., and P.J. Ioannou, 1994: A theory for the statistical equilibrium energy spectrum and heat flux produced by transient baroclinic waves. *J. Atmos. Sci.*, **51**, 2685-2698

Farrell, B.F., and P.J. Ioannou, 1996: Generalized stability theory. Part I: Autonomous operators. *J. Atmos. Sci.*, **53**, 2025-2040

Farrell, B.F., and P.J. Ioannou, 2001: Accurate low-dimensional approximation of the linear dynamics of fluid flow. *J. Atmos. Sci.*, **58**, 2771-2789

Hannachi, A., 1997: Low-frequency variability in a GCM: Three-dimensional flow regimes and their dynamics. *J. Climate* , **10**, 1357-1379

Hasselmann, K., 1988: PIPs and POPs: The reduction of complex dynamical systems using principal interaction and oscillation patterns. *J. Geophys. Res.*, **93**, 11015-11021

Held, I. M., and M. J. Suarez, 1978: A two-level primitive equation atmospheric model designed for climate sensitivity experiments. *J. Atmos. Sci.*, **35**, 206-229

Held, I. M., and M. J. Suarez, 1994: A proposal for the intercomparison of the dynamical cores of atmospheric general circulation models. *Bull. Amer. Meteor. Soc.*, **75**, 1825-1830

Kwasniok, F., 1996: The reduction of complex dynamical systems using principal interaction patterns. *Physica D*, **92**, 28-60

Kwasniok, F., 1997: Optimal Galerkin approximations of partial differential equations using principal interaction patterns. *Phys. Rev. E*, **55**, 5365-5375

Legras, B., and M. Ghil, 1985: Persistent anomalies, blocking and variations in atmospheric predictability. *J. Atmos. Sci.*, **42**, 433-471

Lorenz, E.N., 1963: Deterministic nonperiodic flow. *J. Atmos. Sci.*, **20**, 130-141

Michelangeli, P.-A., R. Vautard, and B. Legras, 1995: Weather regimes: Recurrence and quasi stationarity. *J. Atmos. Sci.*, **52**, 1237-1256

Moise, I., and R. Temam, 2000: Renormalization group method. Application to Navier-Stokes equation. *Discr. Cont. Dyn. Syst.*, **6**, 191-210

Penland, C., and L. Matrosova, 1994: A balance condition for stochastic numerical models with application to the El Nino-Southern Oscillation. *J. Climate*, **7**, 1352-1372

Penland, C., and P.D. Sardeshmukh, 1995: The optimal growth of tropical sea surface temperature anomalies. *J. Climate*, **8**, 1999-2024

Phillips, N.A., 1959: An example of nonlinear computational instability, in *The Atmosphere and Sea in Motion, Rossby Memorial Volume*, Rockefeller Institute Press, New York, 509 pp.

Rinne, J., and V. Karhilla, 1975: A spectral barotropic model in horizontal empirical orthogonal functions. *Quart. J. R. Met. Soc.*, **101**, 365-382

Selten, F.M., 1995: An efficient description of the dynamics of barotropic flow. *J. Atmos. Sci.*, **52**, 915-936

Selten, F.M., 1997a: A statistical closure of a low-order barotropic model. *J. Atmos. Sci.*, **54**, 1085-1093

Selten, F.M., 1997b: Baroclinic empirical orthogonal functions as basis functions in an atmospheric model. *J. Atmos. Sci.*, **54**, 2099-2114

Smagorinsky, J., 1963: General circulation experiments with the primitive equations. I. The basic experiment. *Mon. Wea. Rev.*, **91**, 99-164

Takano, K., and M. G. Wurtele, 1982: A fourth-order energy and potential enstrophy conserving difference scheme. Air Force Geophysics Laboratory Report AFGL-TR-82-0205, AFGL Hanscom AFB, Massachusetts, 01731, 85 pp.

Vautard, R., and B. Legras, 1988: On the source of midlatitude low-frequency variability. Part II: Nonlinear equilibration of weather regimes. *J. Atmos. Sci.*, **45**, 2845-2867

Voss, R., R. Saussen, and U. Cubasch, 1998: Periodically synchronously coupled integrations with the atmosphere-ocean general circulation model ECHAM3/LSG. *Clim. Dyn.*, **14**, 249-266

Whitaker, J.S., and P.D. Sardeshmukh, 1998: A linear theory of extratropical synoptic eddy statistics. *J. Atmos. Sci.*, **55**, 237-258

Zhang, Y., and I.M. Held, 1999: A linear stochastic model of a GCM's midlatitude storm tracks. *J. Atmos. Sci.*, **56**, 3416-3435

Table 1: Newtonian damping parameters used for the semi-empirical models

number of EOFs	A [d^{-1}]	β
10	$8.9 \cdot 10^{-2}$	1.2
20	$2.5 \cdot 10^{-2}$	1.6
30	$2.6 \cdot 10^{-2}$	1.7
40	$2.6 \cdot 10^{-2}$	1.9
50	$2.1 \cdot 10^{-2}$	1.9
60	$2.6 \cdot 10^{-2}$	1.4
100	$6.6 \cdot 10^{-2}$	2.5
200	$1.1 \cdot 10^{-1}$	2.1
500	$3.0 \cdot 10^{-1}$	1.3

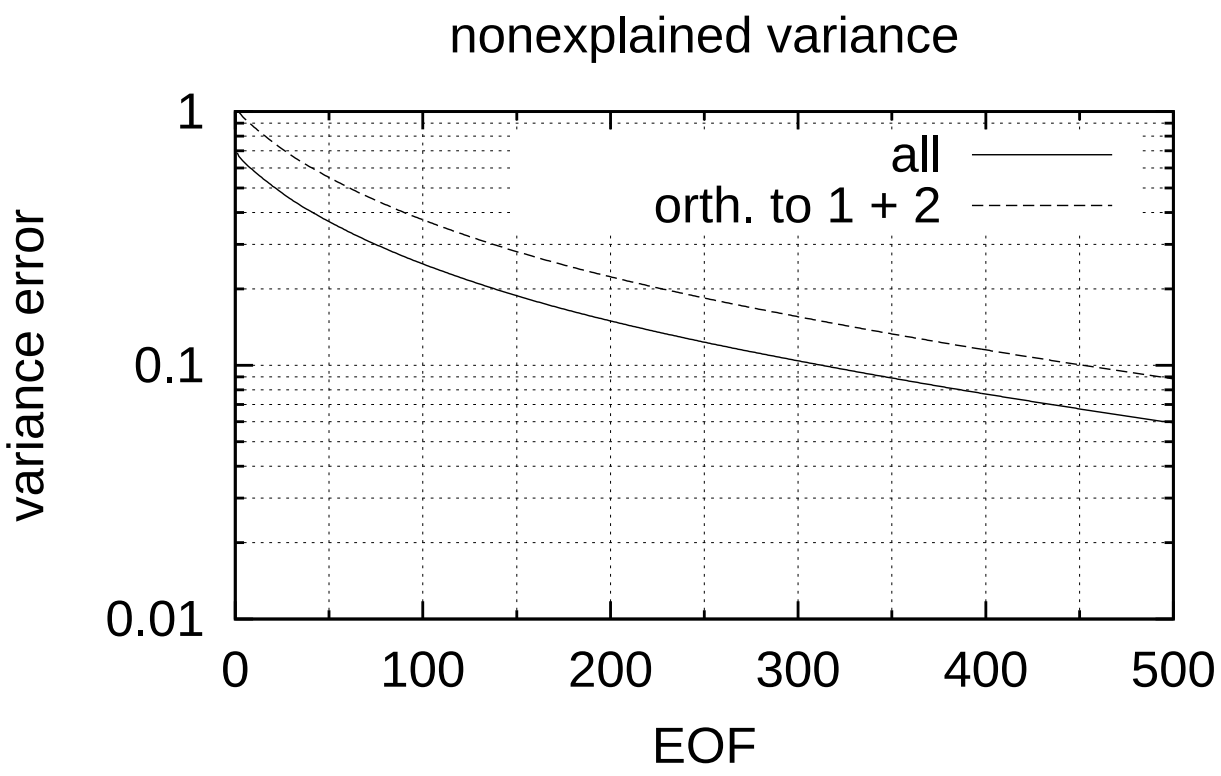

Figure 1: The relative variance not explained by using a given number of global EOFs, for the total variance and the variance orthogonal to the two leading patterns. EOFs 1 and 2 describe most of the seasonal cycle.

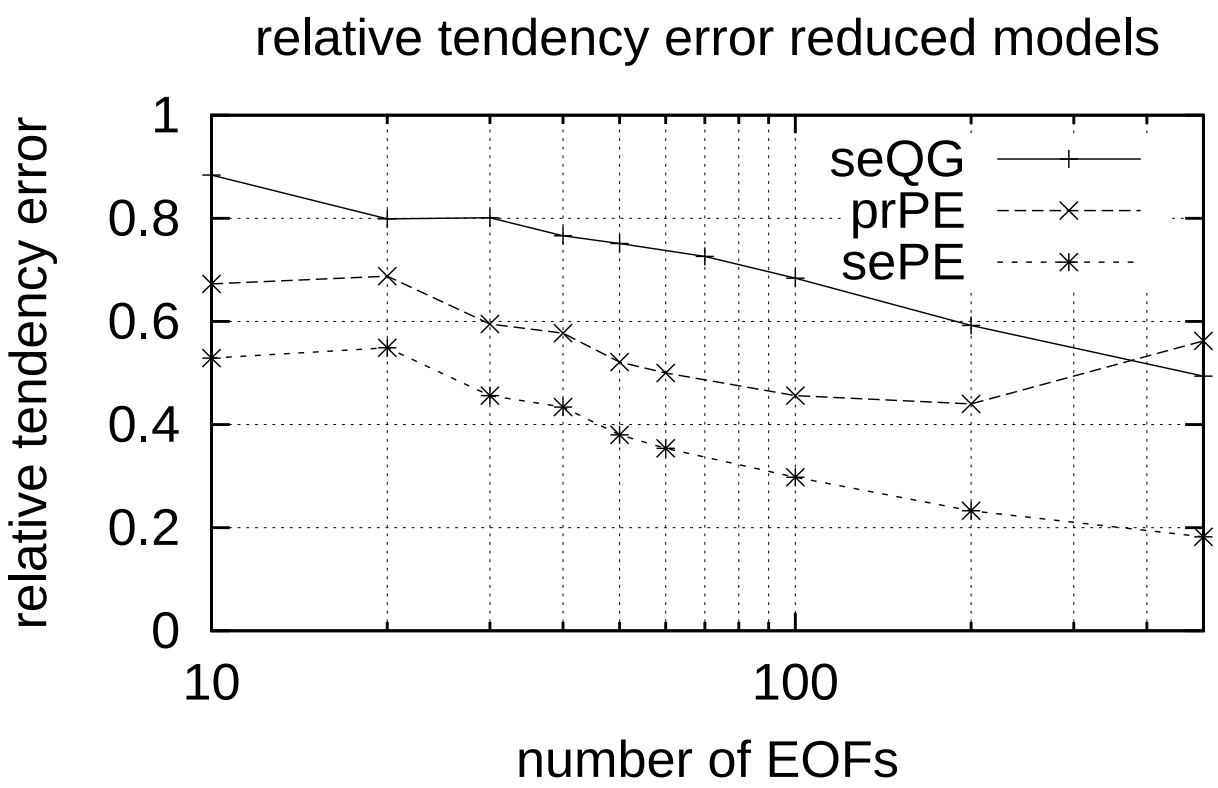

Figure 2: The relative error in the prediction of GCM tendencies (in a data set with seasonal cycle) by the semi-empirical and projected reduced models with primitive equation core, depending on the number of EOFs the model is based on. Also shown are the corresponding results from Achatz and Branstator (1999) for the prediction of tendencies in a perpetual-january data set of a GCM by a semi-empirical reduced model with a quasigeostrophic two-layer model core.

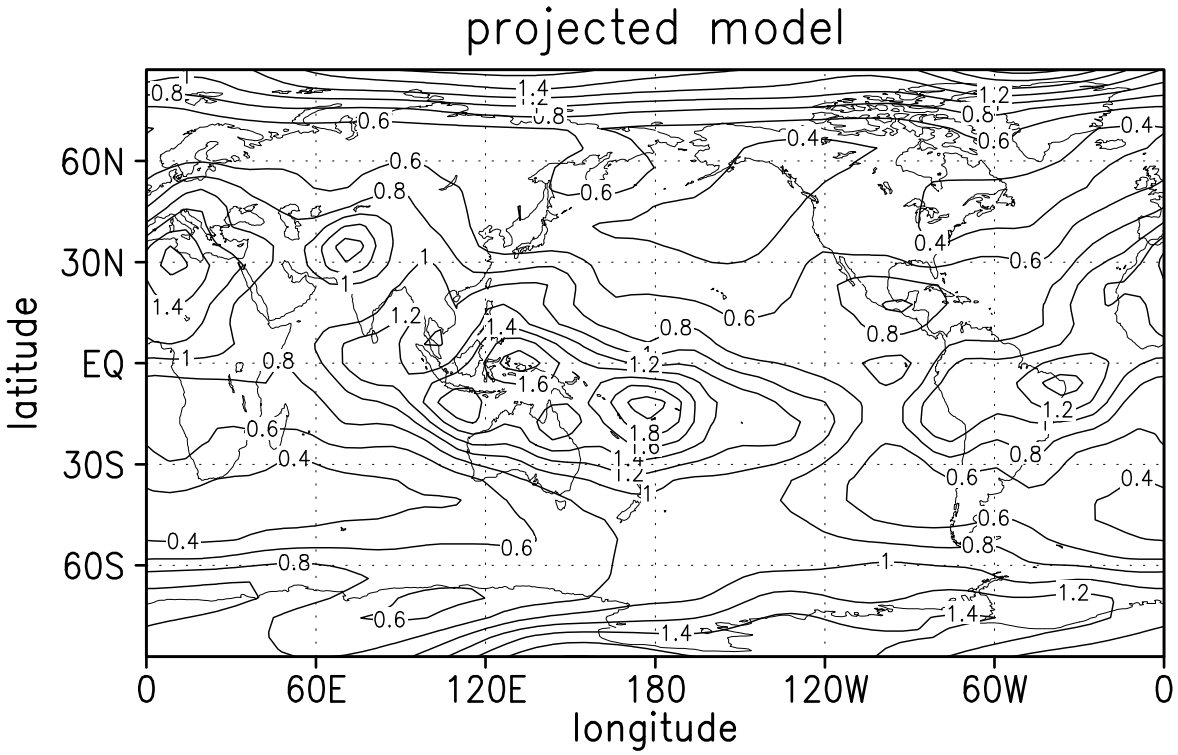

Figure 3: Spatial distribution of the relative (barotropic stream function) tendency error for the projected 500-EOF model. For the comparison both the predicted and the data tendencies (projected onto the leading 500 EOFs) have been tranformed from EOF-representation into grid space where the comparison has been done pointwise. 100 years of data have been taken for the analysis.

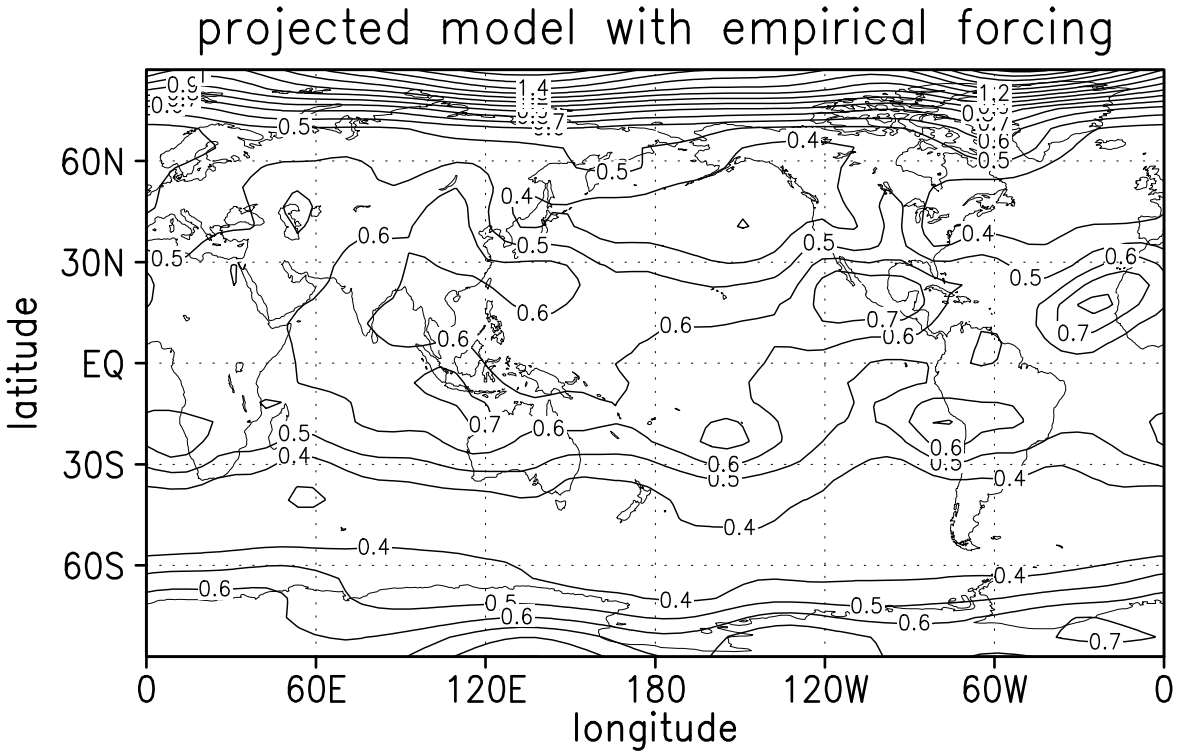

Figure 4: As Fig. 3, but for the projected model with empirical forcing, but without linear closure terms.

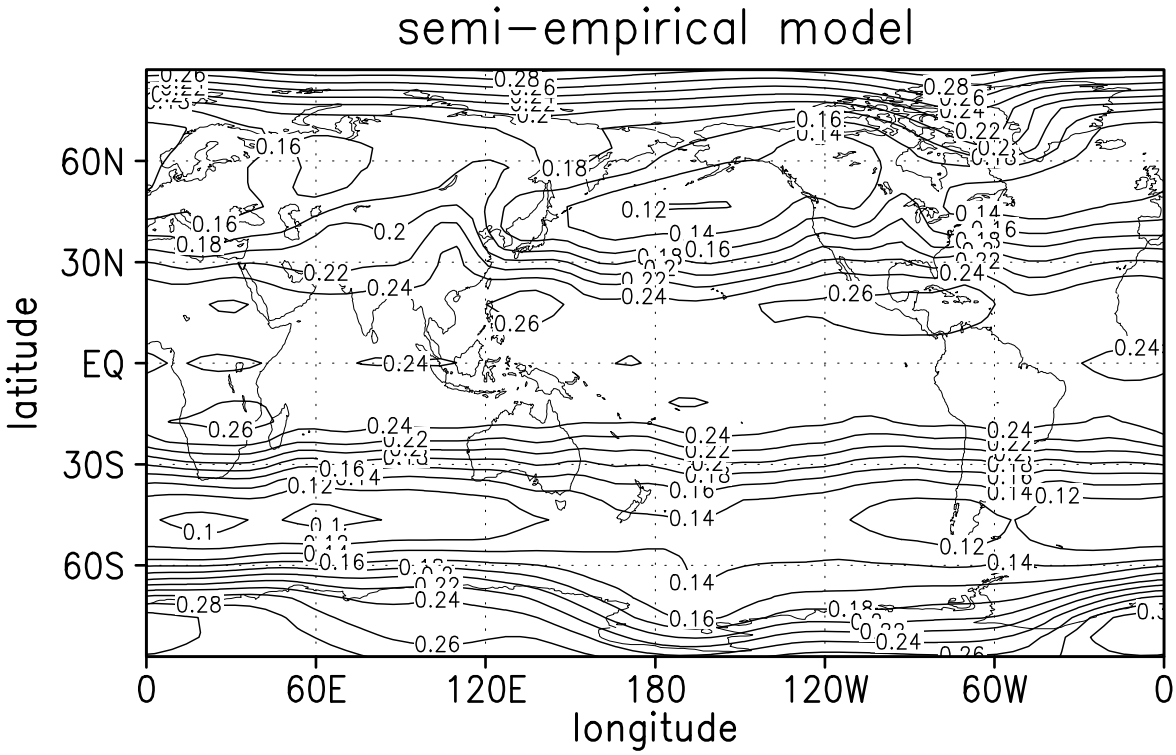

Figure 5: As Fig. 3, but for the complete semi-empirical model (i.e. with empirical forcing and empirical linear corrections).

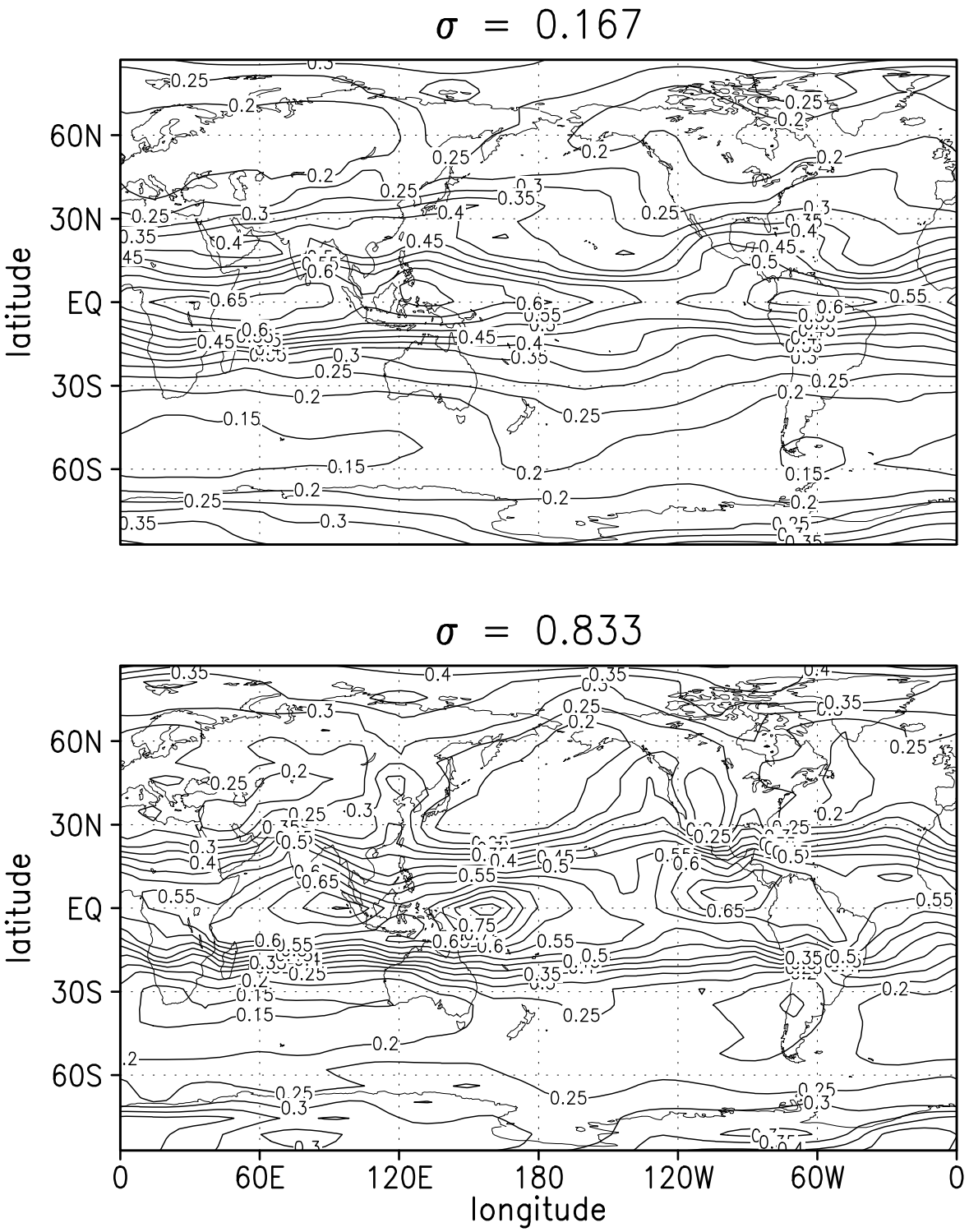

Figure 6: As Fig. 3, but for the relative error made by the complete semi-empirical model in the prediction of zonal wind tendencies. The uppermost and lowermost sigma-levels are shown.

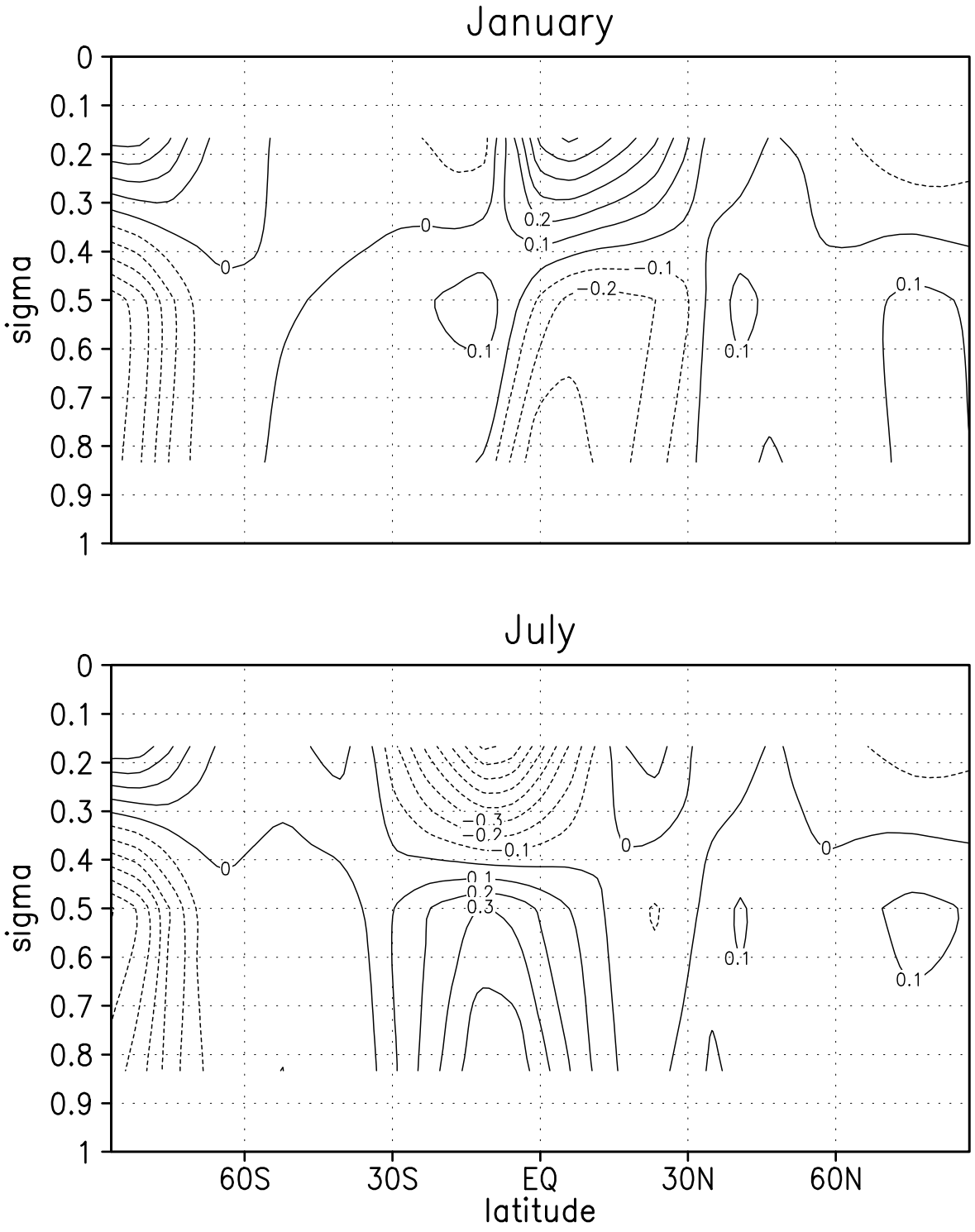

Figure 7: Zonal mean of the empirical meridional-wind forcing in the semi-empirical 500-EOF model in January (top) and July (bottom). Units are $\mathrm{ms}^{-1}\mathrm{d}^{-1}$.

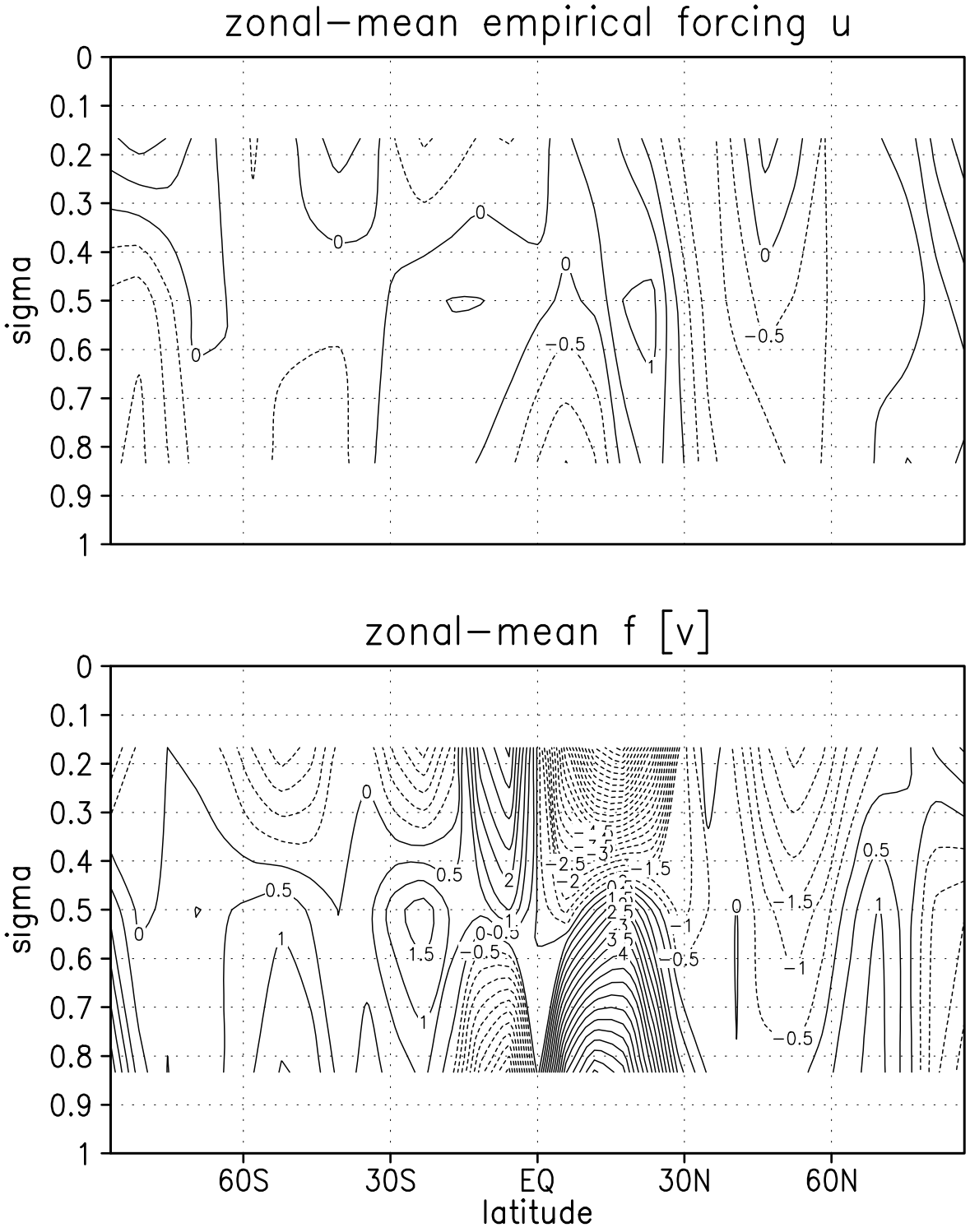

Figure 8: Zonal mean of the empirical zonal-wind forcing in the semi-empirical 500-EOF model in January (top) and the January-mean coriolis term in the zonal-mean zonal-wind equation (bottom). Units are $\mathrm{ms}^{-1}\mathrm{d}^{-1}$.

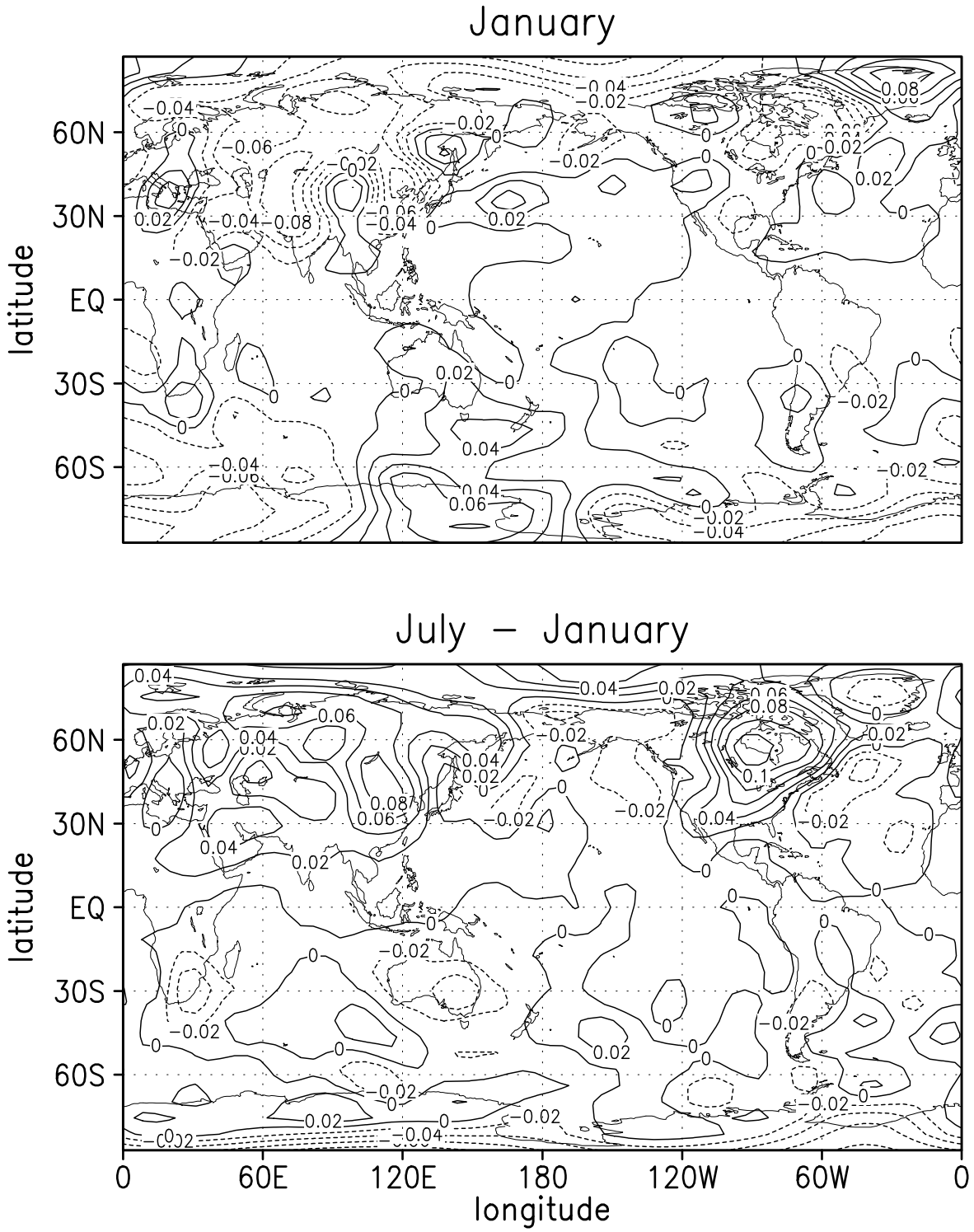

Figure 9: January empirical forcing of the thermodynamic variable τ at $\sigma = 0.833$ in the semi-empirical 500-EOF model (top), and the difference between this and the corresponding field in July (bottom). Units are $\sqrt{\text{K}}\text{d}^{-1}$.

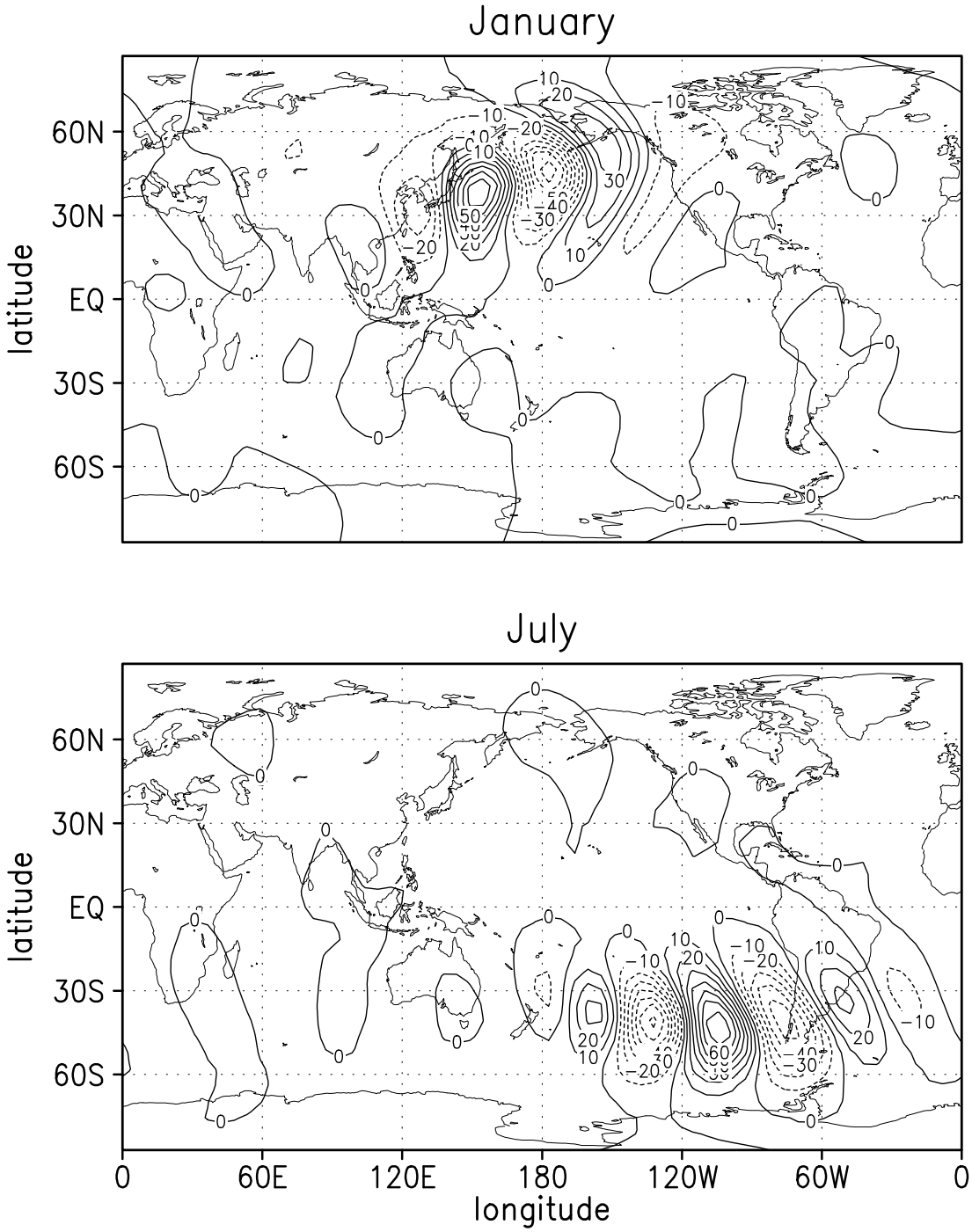

Figure 10: Barotropic-stream-function signature of the January (top) and July (bottom) leading optimal vector for 5-day lead time, obtained by linearizing the semi-empirical 500-EOF model about the respective monthly-mean state of the GCM. The corresponding growth factors are 6.98 in January and 6.21 in July. Units are meaningless.

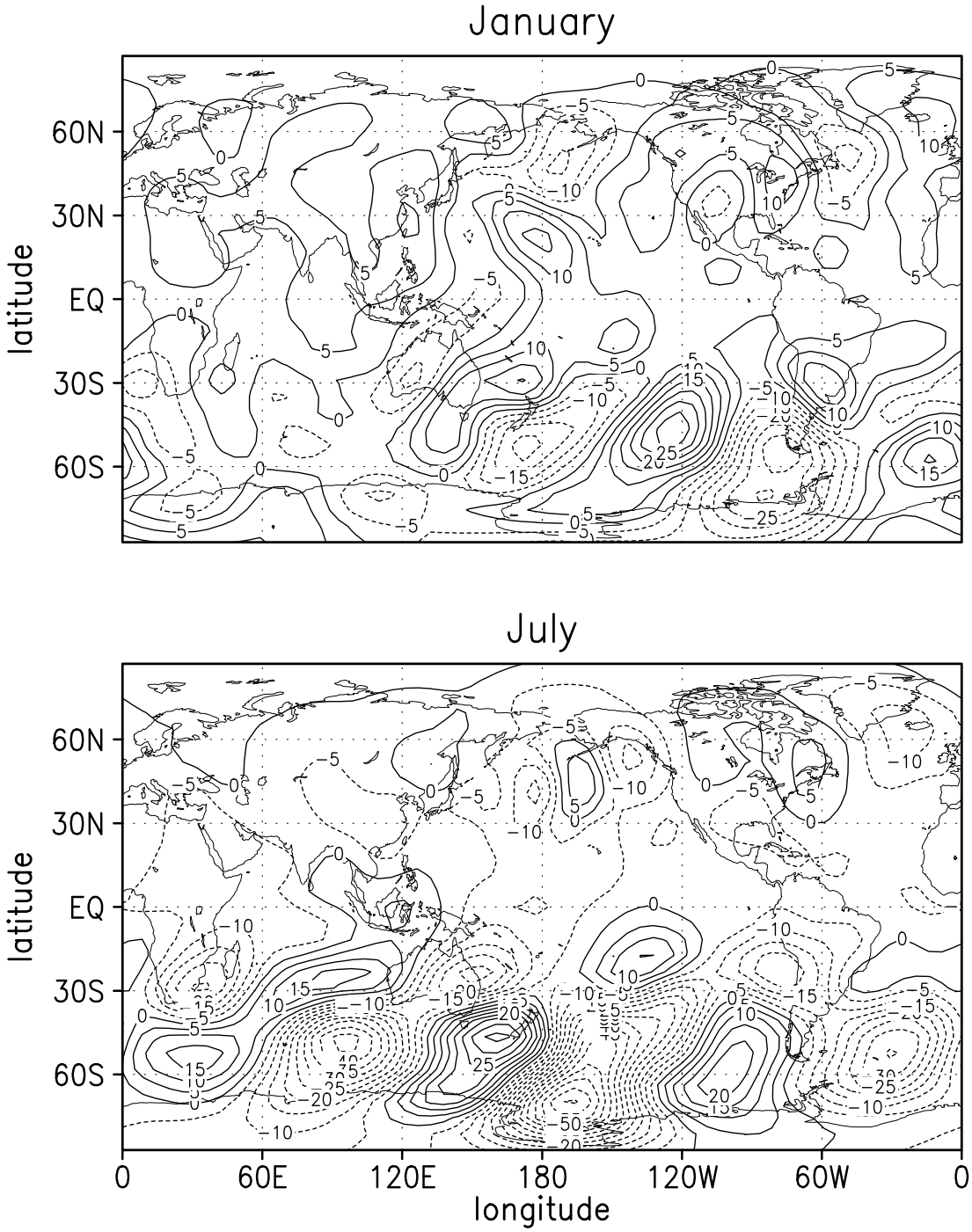

Figure 11: As Fig. 10, but for the 500-EOF model without empirical linear correction.

The January growth factor is 9.46, that for July 9.45.